Nonlinear Dyn (2014) 78:289–315
DOI 10.1007/s11071-014-1440-z

ORIGINAL PAPER

Robust adaptive dynamic surface control design for a flexible air-breathing hypersonic vehicle with input constraints and uncertainty

Qun Zong · Fang Wang · Bailing Tian · Rui Su

Received: 23 October 2013 / Accepted: 29 April 2014 / Published online: 26 May 2014

Abstract The flight control problem of a flexible air-breathing hypersonic vehicle is presented in the presence of input constraint and aerodynamic uncertainty. A control-oriented model, where aerodynamic uncertainty and the strong couplings between the engine and flight dynamics are included, is derived to reduce the complexity of controller design. The flexible dynamics are viewed as perturbations of the model. They are not taken into consideration at the level of control design, the influence of which is evaluated through simulation. The control-oriented model is decomposed into velocity subsystem and altitude subsystem, which are controlled separately. Then robust adaptive controller is developed for the velocity subsystem, while the controller which combines dynamic surface control and radial basis function neural network is designed for the altitude subsystem. The unknown nonlinear function is approximated by the radial basis function neural network. Minimal-learning parameter technique is utilized to estimate the maximum norm of ideal weight vectors instead of their elements to reduce the computational burden. To handle input constraints, additional systems are constructed to analyze their impact, and the states of the additional systems are employed at the level of control design and stability analysis. Besides, "explosion of terms" problem in the traditional backstepping control is circumvented using a first-order filter at each step. By means of Lyapunov stability theory, it is proved theoretically that the designed control law can assure that tracking error converges to an arbitrarily small neighborhood around zero. Simulations are performed to demonstrate the effectiveness of the presented control scheme in coping with input constraint and aerodynamic uncertainty.

Keywords Flexible air-breathing hypersonic vehicle (FAHV) · Dynamic surface control (DSC) · Radial basis function neural network (RBFNN) · Input constraint · Aerodynamic uncertainty

Q. Zong · F. Wang (✉) · B. Tian · R. Su
Department of Electrical Engineering and Automation, Tianjin University, Tianjin 300072, China
e-mail: fangwang@tju.edu.cn

1 Introduction

Since air-breathing hypersonic vehicles (AHVs) are most suitable for prompt global response and offer distinctive air superiority, they have received more and more attention. With the development of hypersonic vehicle technology, there are many challenges for performance requirements of modern hypersonic vehicles. Design of flight control system for AHVs is a challenging task because the dynamics of AHV are complex and highly coupled [1–3]. Much research has been conducted on it [4–11]. For AHV, the engine thrust affects the pitching moment due to the underslung location of scramjet engine. The slender geometry and relative light weight of the vehicle cause the vibration modes to significantly affect the aerodynamic forces. It induces that the vehicle must be viewed as a flex-

ible structure. Moreover, flexible modes may cause adverse aeroservoelastic effects which lead to potential structural damage and instabilities [12]. Flexible effects make control problem more challenging since the flexible modes are uncertain. It is worth noting that the integration of the propulsion system with vehicle and the interactions between the internal and external flow fields make the characteristics of aerodynamics difficult to be measured and estimated. The lack of a broad flight dynamics database suggests that plant parameter variations and uncertainties are the main issues to be addressed at the level of control design [13]. Therefore, the problem about the stability, robustness, and control performance is still the focus of the flexible air-breathing hypersonic vehicle control system. At present, the corresponding data are strictly kept secret since hypersonic vehicle offers a promising technology for cost-efficient access to space and exhibits tremendous and important military merit for its quick response to serious threats around the globe. There is not enough experimental data on both the longitudinal and lateral channels, so the control problem of FAHV focuses on the longitudinal channel. It is important to note that the longitudinal control is very complex. If the longitudinal and lateral channels are taken into account simultaneously, the controller design will become more complex [13]. It is necessary to make a trial between the complexity of the model and the rationality of the controller design under the current technology. More complex model means more states variables, more output variables and stronger nonlinearity, which induces that it is more difficult to design a controller that possesses satisfactory performance. Thus, only the longitudinal analytical model of FAHV proposed in [14] has been applied in the controller design. The control system of FAHV is required to have robustness to tackle uncertainty because of the changeable flight conditions, uncertain aerodynamic characteristics, and highly nonlinear nature dynamics. Aerodynamic uncertainty makes the control system design more difficult.

The flight control system design of FAHV has attracted increasing attention in recent years. Based on modern control techniques, linear and nonlinear control systems have been proposed. The reason why feedback linearization technique could not be applied to design the controller directly for FAHV was analyzed in [15]. Additionally, linear quadratic regulator (LQR) technique was combined with the approximate feedback linearization technique to develop controller to make velocity and altitude track their reference trajectories. In that work, the flexible dynamics and certain dynamic couplings were strategically ignored. A time-varying notch filter algorithm was integrated into trajectory linearization control to address the flight control system design of a hypersonic scramjet vehicle model with flexible modes in [16,17]. Adaptive notch filter and LQ technique were synthesized to design controller in [18], where an adaptive mode suppression scheme accurately tracked and suppressed an unknown or changing flexible mode online. Besides, a robust minimax LQR control scheme was proposed for a control-oriented linearized uncertainty model of a FAHV in [19]. A minimax linear quadratic Gaussian (LQG) control strategy was proposed to solve the control design problem with uncertainties and unmeasured states [20]. However, simulation had been conducted without the flexible dynamics, so the effects of the flexible states cannot be evaluated. The Lyapunov-based robust controller was developed in [21] for a linear-parameter-varying model of FAHV including aerothermoelastic effects and bounded disturbances. Adaptive fuzzy integral sliding mode control scheme was designed for the tracking control problem of a FAHV in the presence of disturbances and possible sensor/actuator failures [22]. Recently, the control design problem of a FAHV was investigated based on adaptive sliding mode control strategy in [23]. Through solving a system of linear algebraic equations, a control approach was presented for a FAHV in [24], in which the suppression of flexible dynamics was achieved by the combination of the control approach with H_∞ control. For the flight path angle and velocity tracking control problem of a FAHV with unmodeled vibration modes, L_1 adaptive control was employed to achieve the stable tracking performance in [25–27]. Adaptive dynamic inversion was combined with nonlinear sequential loop-closure approach to design controller after the system was decomposed into subsystems in [28–30].

Although the research mentioned above achieves good control performance, it is worth pointing out that input constraint is not considered; it usually appears in many practical systems because the amplitudes of control inputs of almost all practical control systems are limited. The closed-loop system performance may be degraded severely or even lose stability if the input constraint is ignored. For the hypersonic vehicle, the flight control system is in open-loop state under the occurrence of input saturation. If the output of actuator

does not return to linear work space, the hypersonic vehicle may lose stability, or even disintegrate. So it is necessary to design the high reliability control system with the consideration of input constraints. In much research, input constraints were not directly taken into account at the level of control design. Instead, they were accounted for manually by tuning the gains to keep the inputs in their valid operating ranges [3]. The presence of unavoidable constraints on the control inputs renders the design of hypersonic vehicle control systems an even harder endeavor [31] except the aforementioned difficulty and challenge. Only few studies are concerned about control problem with control limits owing to the complicated nonlinear dynamics of hypersonic vehicle systems.

An adaptive control strategy was proposed in [32] for reusable launch vehicles (RLVs) with actuator displacement limits, actuator rate limits, linear input dynamics, and time delay, in which input constraints were implemented by pseudocontrol hedging. In [33], for a linear roll/yaw dynamic of an F-16 aircraft, input constraints were addressed by resorting to direct modification of a reference model (μ-modification approach). In [3,34], a flight control system design problem of a FAHV with input constraint was presented through anti-windup control (AWC), but aerodynamic uncertainty was not considered. In [31], a control problem with a constraint on the fuel equivalence ratio was addressed by a plug-in approach, where a self-optimizing guidance scheme shaped the reference to be tracked. It assured that the input constraints were not violated to an adaptive guidance system. Model predictive control has been used popularly because of its inherent capability to implement input constraint directly at the level of control design [35–37]. However, it depends on the real-time receding horizon optimization, and the main barrier of its application to hypersonic vehicle is online optimization and the determination of time-domain step size [38]. Furthermore, some other methods had been employed to design controller of FAHV. H_∞ approach was proposed for a linearized model of FAHV with input constraints, in which the linearized model with uncertain parameters was obtained by the feedback linearization technique [39]. It should be pointed out that high-order derivatives of outputs need to be computed. Advanced flight control laws concerned with actuator limitations were designed for hypersonic vehicle using the differential geometry principle and the total energy theory [40]. Three adaptive fault control schemes were proposed for tracking control problem of an AHV with external disturbances, actuator faults, and input saturation in [41]. For the latter two control approaches, there was no need to know the upper bound of the external disturbances and the real minimum value of actuator efficiency factor in advance.

As a powerful nonlinear technique, backstepping control has also been used for control system design with input constraints. In [42], an adaptive backstepping approach was applied to flight control system design of longitudinal aircraft dynamics that directly accommodated magnitude, rate, and bandwidth limits on aircraft states and actuators. However, external disturbance was not considered. For F-16/MATV (multi-axis thrust vectoring) aircraft control problem, a constrained adaptive backstepping control scheme was proposed where command filters implemented constraints on control surfaces and virtual control states [43]. The constraints were handled by command filters. The designed approach retained that the state and control constraints could be enforced while maintaining Lyapunov stability. In [44], an adaptive backstepping controller was proposed for RLV with input constraint and external disturbance, in which the bound of external disturbance and uncertainty was estimated and updated by adaptive law. It is well known that "explosion of terms" problem inherent in traditional backstepping control constrains the application of backstepping to an extent. Dynamic surface control (DSC) was presented to overcome it, where the synthetic input at each step of backstepping procedure was filtered by a first-order filter. In [45], an adaptive dynamic surface controller was proposed for a generic hypersonic flight vehicle with consideration of actuator constraints including accommodation on magnitude, rate, and bandwidth constraints on actuator signals. To improve tracking performance of the designed controller, a novel integral term was introduced during DSC scheme design procedure to avoid a large initial control signal [46]. The magnitude and rate constraints on the actuator commands were taken into consideration to ensure feasibility. Moreover, a robust adaptive dynamic surface controller was investigated for a hypersonic vehicle in the presence of parametric model uncertainty and input saturation. A compensation design was employed when the input saturations occurred [47]. Air speed and flight path angle control problem of a generic hypersonic flight vehicle was studied in [48], where

magnitude, rate, and bandwidth constraints on actuator were considered. In that research, an adaptive DSC scheme based on radial basis function neural network (RBFNN) was presented. Furthermore, nonlinear disturbance observer and RBFNN were integrated into sliding mode control to design controller for a near space vehicle in [49]. Considering saturation characteristic of rudders, RBFNN was constructed as a compensator to avoid the saturation nonlinearity.

The motivation of this paper is to develop a nonlinear robust adaptive dynamic surface controller for FAHV based on RBFNN to achieve stable tracking of velocity and altitude reference commands, in which both uncertain aerodynamic parameters and input constraint are accommodated. The contribution can be summarized as follows. Firstly, a nonlinear control-oriented model (COM) is firstly derived from a curved-fitted model. It does not need to obtain a linearized model at a trim condition or to compute the higher-order derivatives of outputs. The flexible dynamics are regarded as the perturbations of COM and evaluated by simulation. The strong couplings between the engine and flight dynamics are kept in COM. The uncertainty of aerodynamic parameters is considered. What is more, compared with the existing results, most of which consider the interconnect gain between canard deflection and elevator deflection certain (i.e., the canard would exactly cancel the lift due to the elevator deflection); in this paper, the interconnect gain is regarded as an uncertain variable from the engineering point. Based on the analysis of the COM, it is reasonable to decompose it into velocity subsystem and altitude subsystem. Secondly, the subsystems are controlled separately by the available control inputs (fuel equivalence ratio and elevator deflection). The RBFNN is employed to approximate unknown nonlinear function. The RBFNN-based robust adaptive controller is designed for the velocity subsystem. The altitude subsystem comprised the dynamic equations of altitude, flight- path angle, angle of attack, and pitch rate. The RBFNN-based robust adaptive dynamic surface controller is designed after it is transformed into pure-feedback formulation. During the controller design procedure, a minimal-learning parameter (MLP) technique is used to estimate the maximum norm of the ideal weight vectors of RBFNN rather than their elements. The computational burden is largely reduced. Thirdly, by applying the first-order filters at the level of control design, "explosion of terms" problem induced by the repeated derivative of virtual control inputs is avoided. To tackle input constraints, the respective additional systems are established to analyze their influence. States of the additional systems are employed at the level of control design and stability analysis. Fourthly, stability analysis of the rigid body system is performed on the basis of Lyapunov theory, and boundedness of the flexible states is demonstrated through simulation. Moreover, compared simulations are done to present effectiveness of the designed control scheme in handling input constraints and aerodynamic uncertainty.

The rest of the paper is organized as follows. In Sect. 2, the vehicle model and the researched problem are formulated. In Sect. 3, a nonlinear controller is developed for the COM with input constraint and aerodynamic uncertainty based on RBFNN and robust adaptive dynamic surface control. Then in Sect. 4, the stability of rigid body system is analyzed based on Lyapunov theory. Simulation results and analysis are presented in Sect. 5. The paper ends with conclusions in Sect. 6.

2 Vehicle model

The model adopted in the paper is originated from a first principles model developed in [1,14]. It is constructed for longitudinal dynamics of a FAHV. A sketch of the vehicle geometry showing the location of control surfaces is given in Fig. 1, which is according to [50]. The equations of motion derived using Lagrange's equations which include flexible effects by modeling the vehicle as a single flexible structure with mass-normalized mode shapes. In the equations of motion, the scramjet engine model is taken from [51]. Since aerodynamic forces and moments are calculated using oblique shock and Prandtl–Meyer theory, relation between control inputs and controlled outputs does not admit a closed-form representation. A simplified model has been derived for controller design and stability analysis in [50]. This model, called as a curve-fitted model (CFM), approximates behavior of the first principles model by replacing the aerodynamic and generalized forces and moments with curve-fitted functions of rigid body states, control inputs, and flexible modes. Though the resulting nonlinear model is still quite complex, it offers the advantage of being analytically tractable while retaining relevant dynamical features of the first principles model.

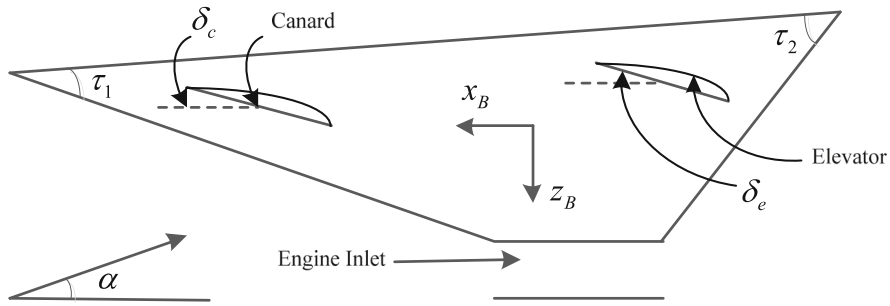

Fig. 1 Geometry of an air-breathing hypersonic vehicle

The longitudinal dynamic equations of a FAHV, which describe five rigid body states velocity V, altitude h, flight path angle (FPA) γ, angle of attack (AOA) α, pitch rate Q, and six flexible states η_1, η_2, η_3, $\dot{\eta}_1$, $\dot{\eta}_2$, and $\dot{\eta}_3$ are given as

$$\dot{V} = (T\cos\alpha - D)/m - g\sin\gamma, \tag{1}$$
$$\dot{h} = V\sin\gamma, \tag{2}$$
$$\dot{\gamma} = (L + T\sin\alpha)/(mV) - g\cos\gamma/V, \tag{3}$$
$$\dot{\alpha} = Q - \dot{\gamma}, \tag{4}$$
$$\dot{Q} = M_{yy}/I_{yy}, \tag{5}$$
$$\ddot{\eta}_i = -2\xi_i\omega_i\dot{\eta}_i - \omega_i^2\dot{\eta}_i + N_i, i = 1, 2, 3. \tag{6}$$

In Eqs. (1)–(6), the thrust T, drag D, lift L, pitching moment M_{yy}, and three generalized forces N_1, N_2, and N_3 are complex algebraic functions of both the system states and inputs that must be simplified to render the model analytically tractable. Flexible states η_1, η_2, η_3, $\dot{\eta}_1$, $\dot{\eta}_2$, and $\dot{\eta}_3$ are corresponding to the first three vibrational modes. The damping ratio and natural frequency of the mass-normalized generalized coordinates of the flexible structure are denoted by ξ_i and ω_i, respectively. The flexible states η_1, η_2, and η_3 are related to the deflections of the fore-body turn angle τ_1 and aft-body vertex angle τ_2, denoted by $\Delta\tau_1$ and $\Delta\tau_2$, respectively. The vector $\eta = [\eta_1, \eta_2, \eta_3]^T$ and the matrix $E_j \in R^{1\times 3}$ depend on the fuel level. They describe the relationship $\Delta\tau_j = E_j\eta$, $j = 1, 2$. Approximations of the forces and moments are the same as those provided in [50], which can be expressed as

$$\begin{aligned}
&T \approx \overline{q}[\phi\, C_{T,\phi}(\alpha, \Delta\tau_1, M_\infty) + C_T(\alpha, \Delta\tau_1, M_\infty, A_d)],\\
&D \approx \overline{q}SC_D(\alpha, \delta_e, \delta_c, \Delta\tau_1, \Delta\tau_2),\\
&L \approx \overline{q}SC_L(\alpha, \delta_e, \delta_c, \Delta\tau_1, \Delta\tau_2),\\
&M_{yy} \approx z_T T + \overline{q}S\overline{c}C_M(\alpha, \delta_e, \delta_c, \Delta\tau_1, \Delta\tau_2),\\
&N_i \approx \overline{q}C_{N_i}(\alpha, \delta_e, \delta_c, \Delta\tau_1, \Delta\tau_2),\ i = 1, 2, 3.
\end{aligned} \tag{7}$$

Here, M_∞ is free stream Mach number and $\overline{q}$ is dynamic pressure. They are defined as $\overline{q} = 0.5\rho(h)V^2$, $M_\infty = V/M_0.\rho(h)$ is the altitude-dependent air density, and M_0 is the speed of sound at a given altitude and temperature. The coefficients obtained from fitting the curves are given below; here, the function arguments are removed in brief:

$$\begin{aligned}
C_{T,\phi} &= C_{T,\phi}^{\alpha}\alpha + C_{T,\phi}^{\alpha M_\infty^{-2}}\alpha M_\infty^{-2} + C_{T,\phi}^{\alpha\,\Delta\tau_1}\alpha\Delta\tau_1\\
&\quad + C_{T,\phi}^{M_\infty^{-2}}M_\infty^{-2} + C_{T,\phi}^{\Delta\tau_1^2}\Delta\tau_1^2 + C_{T,\phi}^{\Delta\tau_1}\Delta\tau_1 + C_{T,\phi}^{0},\\
C_T &= C_T^{A_d}A_d + C_T^{\alpha}\alpha + C_T^{M_\infty^{-2}}M_\infty^{-2} + C_T^{\Delta\tau_1}\Delta\tau_1 + C_T^{0},\\
C_D &= C_D^{(\alpha+\Delta\tau_1)^2}(\alpha+\Delta\tau_1)^2 + C_D^{(\alpha+\Delta\tau_1)}(\alpha+\Delta\tau_1)\\
&\quad + C_D^{\delta_e^2}\delta_e^2 + C_D^{\delta_e}\delta_e\\
&\quad + C_D^{\delta_c^2}\delta_c^2 + C_D^{\delta_c}\delta_c + C_D^{\alpha\delta_e}\alpha\delta_e + C_D^{\alpha\delta_c}\alpha\delta_c\\
&\quad + C_D^{\Delta\tau_2}\Delta\tau_2 + C_D^{0},\\
C_L &= C_L^{\alpha}\alpha + C_L^{\delta_e}\delta_e + C_L^{\delta_c}\delta_c + C_L^{\Delta\tau_1}\Delta\tau_1\\
&\quad + C_L^{\Delta\tau_2}\Delta\tau_2 + C_L^{0},\\
C_M &= C_M^{\alpha}\alpha + C_M^{\delta_e}\delta_e + C_M^{\delta_c}\delta_c\\
&\quad + C_M^{\Delta\tau_1}\Delta\tau_1 + C_M^{\Delta\tau_2}\Delta\tau_2 + C_M^{0},\\
C_{N_i} &= C_{N_i}^{\alpha}\alpha + C_{N_i}^{\delta_e}\delta_e + C_{N_i}^{\delta_c}\delta_c + C_{N_i}^{\Delta\tau_1}\Delta\tau_1\\
&\quad + C_{N_i}^{\Delta\tau_2}\Delta\tau_2 + C_{N_i}^{0}.
\end{aligned} \tag{8}$$

The flexible states η_1, η_2, η_3, $\dot{\eta}_1$, $\dot{\eta}_2$, and $\dot{\eta}_3$ correspond to the first three bending modes of the fuselage. It is obvious from (7) to (8) that the interaction between rigid body and flexible dynamics occurs through the aerodynamic forces. The aerodynamic forces/moments and the generalized elastic forces are influenced by $\Delta\tau_1$, $\Delta\tau_2$ and the aerodynamic control surfaces δ_e, δ_c as shown in coefficient formulation (8). Flexible modes may cause adverse aeroservoelastic effect degrading performance which induces potential structural dam-

age and instabilities. What is more, the aerothermodynamic effects of the hypersonic speed, and strong interaction between the elastic airframe, the propulsion system, and the structural dynamics make it challenging to explicit the characterization of flight dynamics of FAHVs [52–54].

2.1 Control-oriented model

The CFM described in the above subsection is only used for simulation. A simplified model, called control-oriented model (COM), is derived for controller design as discussed in [15,28,29]. The CFM is obtained by neglecting the flexible dynamics for the measurements of the flexible states are not assumed to be available for feedback [30]. Regardless of the fact that the flexible dynamics are not considered directly at the level of control design, their effects are taken as perturbations of the COM and evaluated in the simulation. The COM is composed of five rigid body dynamic equations. The COM retains all the dominant features of the CFM, including flexible effects ($\Delta\tau_1$ and $\Delta\tau_2$) and coupled propulsive and aerodynamic forces.

It is noted that in the COM a canard is used to cancel lift–elevator coupling. Canard deflection δ_c is a function of the elevator deflection δ_e so that $\delta_c = k_{ec}\delta_e$, where $k_{ec} = -C_L^{\delta_e}/C_L^{\delta_c}$, is an interconnect gain [15,28]. From the lift coefficient in (8), it is obvious that if k_{ec} is precisely specified, the canard would exactly cancel the lift due to the elevator deflection. However, in practice, it is difficult to achieve an ideal interconnect gain. It is impossible to obtain the exact cancellation of the lift–elevator coupling. Hence, it is reasonable to assume that $k_{ec} = k_{ec0} + \Delta k_{ec}$ is uncertain. The product of its uncertain part Δk_{ec} and elevator deflection δ_e, i.e., $\Delta k_{ec}\delta_e$, is an uncertain term with a bound on its magnitude and satisfies an integral quadratic constraint condition [19,55].

Based on what is mentioned above, the expression for C_L is written as

$$C_L = C_L^{\alpha}\alpha + C_L^0 + C_L^{\delta_c}\Delta k_{ec}\delta_e + C_L^{\Delta\tau_1}\Delta\tau_1 + C_L^{\Delta\tau_2}\Delta\tau_2. \tag{9}$$

Similarly, the drag coefficient C_D is also affected by this coupling owing to the presence of an elevator, canard, and AOA cross- coupling terms in the corresponding expression. These coupling terms are modeled as an uncertainty ΔC_d with a bound on its magnitude and it satisfies an integral quadratic constraint condition [19]. The expression C_D is given as

$$\begin{aligned} C_D = {} & C_D^{(\alpha+\Delta\tau_1)^2}\alpha^2 + C_D^{(\alpha+\Delta\tau_1)}\alpha \\ & + C_D^0 + C_D^{(\alpha+\Delta\tau_1)^2}(2\alpha\Delta\tau_1 + \Delta\tau_1^2) \\ & + C_D^{(\alpha+\Delta\tau_1)}\Delta\tau_1 + C_D^{\Delta\tau_2}\Delta\tau_2 + \Delta C_d, \end{aligned} \tag{10}$$

with $\Delta C_d = [C_D^{\delta_e^2} + (k_{ec0} + \Delta k_{ec})^2 C_D^{\delta_c^2}]\delta_e^2 + [C_D^{\delta_e} + C_D^{\delta_c}(k_{ec0} + \Delta k_{ec})]\delta_e + [C_D^{\alpha\delta_e} + C_D^{\alpha\delta_c}(k_{ec0} + \Delta k_{ec})]\alpha\delta_e$.

By the same token, the expressions of C_M and C_{N_i} are given as

$$\begin{aligned} C_M = {} & C_M^{\alpha}\alpha + (C_M^{\delta_e} + C_M^{\delta_c}k_{ec0} + C_M^{\delta_c}\Delta k_{ec})\delta_e \\ & + C_M^0 + C_M^{\Delta\tau_1}\Delta\tau_1 + C_M^{\Delta\tau_2}\Delta\tau_2, \end{aligned} \tag{11}$$

$$\begin{aligned} C_{N_i} = {} & C_{N_i}^{\alpha}\alpha + (C_{N_i}^{\delta_e} + C_{N_i}^{\delta_c}k_{ec0} + C_{N_i}^{\delta_c}\Delta k_{ec})\delta_e \\ & + C_{N_i}^0 + C_{N_i}^{\Delta\tau_1}\Delta\tau_1 + C_{N_i}^{\Delta\tau_2}\Delta\tau_2. \end{aligned} \tag{12}$$

In this study, the mass of the vehicle m, which varies due to fuel consumption on a slower time scale with respect to the references to be tracked, will be considered constant during each tracking maneuver as all the other model parameters [29]. But the following uncertain aerodynamic parameters are considered, k_{ec0}, C_L^{α}, $C_L^0, C_L^{\Delta\tau_1}, C_L^{\Delta\tau_2}, C_D^{(\alpha+\Delta\tau_1)^2}, C_D^{(\alpha+\Delta\tau_1)}, C_D^{\Delta\tau_2}, C_D^0, C_D^{\delta_e^2}$, $C_D^{\delta_c^2}, C_D^{\delta_e}, C_D^{\delta_c}, C_D^{\alpha\delta_e}, C_D^{\alpha\delta_c}, C_M^{\alpha}, C_M^{\delta_e}, C_M^{\delta_c}, C_M^0, C_M^{\Delta\tau_1}$, $C_M^{\Delta\tau_2}, C_{T,\phi}^{\alpha}, C_{T,\phi}^{\alpha M_\infty^{-2}}, C_{T,\phi}^{\alpha\Delta\tau_1}, C_{T,\phi}^{M_\infty^{-2}}, C_{T,\phi}^{\Delta\tau_1^2}, C_{T,\phi}^{\Delta\tau_1}, C_{T,\phi}^0$, $C_T^{A_d}, C_T^{\alpha}, C_T^{M_\infty^{-2}}, C_T^{\Delta\tau_1}, C_T^0, C_{N_i}^{\alpha}, C_{N_i}^{\delta_e}, C_{N_i}^{\delta_c}, C_{N_i}^{\Delta\tau_1}, C_{N_i}^{\Delta\tau_2}$, $C_{N_i}^0$. The uncertainty of aerodynamic parameter C_L^{α} is denoted as ΔC_L^{α}. Based on it, we can obtain the expressions about the uncertainty of aerodynamic parameters as follows

$$\begin{aligned} \Delta C_L = {} & \Delta C_L^{\alpha}\alpha + \Delta C_L^0 + \Delta C_L^{\Delta\tau_1}\Delta\tau_1 \\ & + \Delta C_L^{\Delta\tau_2}\Delta\tau_2 + C_L^{\delta_c}\Delta k_{ec}\delta_e, \end{aligned} \tag{13}$$

$$\begin{aligned} \Delta C_D = {} & \Delta C_D^{(\alpha+\Delta\tau_1)^2}(\alpha+\Delta\tau_1)^2 + \Delta C_D^{(\alpha+\Delta\tau_1)}(\alpha+\Delta\tau_1) \\ & + \Delta C_D^{\Delta\tau_2}\Delta\tau_2 + \Delta C_D^0 + \Delta C_d, \end{aligned} \tag{14}$$

where

$$\begin{aligned} \Delta C_d = {} & [\Delta C_D^{\delta_e^2} + (k_{ec0} + \Delta k_{ec})^2\Delta C_D^{\delta_c^2}]\delta_e^2 \\ & + [\Delta C_D^{\delta_e} + \Delta C_D^{\delta_c}(k_{ec0} + \Delta k_{ec})]\delta_e \\ & + [\Delta C_D^{\alpha\delta_e} + \Delta C_D^{\alpha\delta_c}(k_{ec0} + \Delta k_{ec})]\alpha\delta_e, \\ \Delta C_M = {} & \Delta C_M^{\alpha}\alpha + [\Delta C_M^{\delta_e} + \Delta C_M^{\delta_c}(k_{ec0} + \Delta k_{ec})]\delta_e \\ & + \Delta C_M^{\Delta\tau_1}\Delta\tau_1 + \Delta C_M^{\Delta\tau_2}\Delta\tau_2 + \Delta C_M^0, \end{aligned}$$

$$\begin{aligned}\Delta C_{T,\phi} &= \Delta C_{T,\phi}^{\alpha}\alpha + \Delta C_{T,\phi}^{\alpha M_\infty^{-2}}\alpha M_\infty^{-2} + \Delta C_{T,\phi}^{M_\infty^{-2}} M_\infty^{-2} \\ &\quad + \Delta C_{T,\phi}^{0} + \Delta C_{T,\phi}^{\alpha\,\Delta\tau_1}\alpha\Delta\tau_1 + \Delta C_{T,\phi}^{\Delta\tau_1^2}\Delta\tau_1^2 \\ &\quad + \Delta C_{T,\phi}^{\Delta\tau_1}\Delta\tau_1, \\ \Delta C_T &= \Delta C_T^{A_d} A_d + \Delta C_T^{\alpha}\alpha + \Delta C_T^{M_\infty^{-2}} M_\infty^{-2} \\ &\quad + \Delta C_T^{\Delta\tau_1}\Delta\tau_1 + \Delta C_T^{0}, \\ C_{N_i} &= \Delta C_{N_i}^{\alpha}\alpha + (\Delta C_{N_i}^{\delta_e} v + \Delta C_{N_i}^{\delta_c} k_{ec0} + \Delta C_{N_i}^{\delta_c}\Delta k_{ec})\delta_e \\ &\quad + \Delta C_{N_i}^{0} + \Delta C_{N_i}^{\Delta\tau_1}\Delta\tau_1 + \Delta C_{N_i}^{\Delta\tau_2}\Delta\tau_2, i = 1, 2, 3. \\ \Delta L &\approx \overline{q}S\Delta C_L,\ \Delta D \approx \overline{q}S\Delta C_D, \Delta M_{yy} \approx z_T\Delta T \\ &\quad + \overline{q}S\overline{c}\Delta C_M, \Delta T \\ &= \overline{q}(\phi\,\Delta C_{T,\phi} + \Delta C_T), \Delta N_i \approx \overline{q}\Delta C_{N_i}.\end{aligned} \tag{15}$$

It is worthy to point out that in the vehicle model (1)–(5) and aerodynamic formulation (7), thrust T affects velocity V and fuel equivalence ratio ϕ, so the velocity is mainly affected by ϕ. Moreover, elevator deflection δ_e has a dominant contribution to the altitude h change. Therefore, it is reasonable to implement a separate control design. So the equations of motion of the COM are reasonably decomposed into velocity subsystem and altitude subsystem.

Considering the aerodynamic uncertainty, the dynamic of velocity (1) can be expressed as the following form

$$\dot{V} = f_V + g_V\phi, \tag{16}$$

where

$$\begin{aligned}f_V &= f_{V0} + \Delta f_V, g_V = \overline{q}\,C_{T,\phi,1}\cos\alpha/m, C_{T,\phi,1} \\ &= C_{T,\phi}^{\alpha}\alpha + C_{T,\phi}^{\alpha M_\infty^{-2}}\alpha M_\infty^{-2} + C_{T,\phi}^{M_\infty^{-2}} M_\infty^{-2} + C_{T,\phi}^{0}, \\ f_{V0} &= \overline{q}C_{T,1}\cos\alpha/m - g\sin\gamma \\ &\quad - \overline{q}S(C_D^{(\alpha+\Delta\tau_1)^2}\alpha^2 + C_D^{(\alpha+\Delta\tau_1)}\alpha + C_D^{0})/m, \\ \Delta f_V &= \Big[\Delta T + \overline{q}\phi(C_{T,\phi}^{\alpha\,\Delta\tau_1}\alpha\Delta\tau_1 + C_{T,\phi}^{\Delta\tau_1^2}\Delta\tau_1^2 \\ &\quad + C_{T,\phi}^{\Delta\tau_1}\Delta\tau_1) + \overline{q}C_T^{\Delta\tau_1}\Delta\tau_1\Big]\cos\alpha/m \\ &\quad - \Big[D - \overline{q}S(C_D^{(\alpha+\Delta\tau_1)^2}\alpha^2 + C_D^{\alpha+\Delta\tau_1}\alpha \\ &\quad + C_D^{0}) + \Delta D\Big]/m, \\ C_{T,1} &= C_T^{A_d}A_d + C_T^{\alpha}\alpha + C_T^{M_\infty^{-2}}M_\infty^{-2} + C_T^{0}.\end{aligned}$$

Similarly, the dynamics of FPA, AOA, and pitch rate are rewritten as the following form:

$$\dot{\gamma} = f_\gamma(\gamma,\alpha) + g_\gamma(\alpha)\alpha, \tag{17}$$

$$\dot{\alpha} = f_\alpha(\gamma,\alpha,Q) + g_\alpha Q, \tag{18}$$

$$\dot{Q} = f_Q(\gamma,\alpha,Q) + g_Q\delta_e, \tag{19}$$

where

$$\begin{aligned}f_\gamma(\gamma,\alpha) &= f_{\gamma 0}(\gamma,\alpha) + \Delta f_\gamma(\gamma,\alpha), \\ f_{\gamma 0}(\gamma,\alpha) &= \overline{q}\phi\sin\alpha\Big[(C_{T,\phi}^{M_\infty^{-2}}M_\infty^{-2} + C_{T,\phi}^{0})\Big]\Big/ \\ &\quad (mV) - g\cos\gamma/(mV) \\ &\quad + \overline{q}\sin\alpha\Big[(C_T^{A_d}A_d + C_T^{\alpha}\alpha + C_T^{0} \\ &\quad + C_T^{M_\infty^{-2}}M_\infty^{-2}) + \overline{q}SC_L^{0}\Big]\Big/(mV), \\ \Delta f_\gamma(\gamma,\alpha) &= \Big[\Delta T + \overline{q}\phi\Big(C_{T,\phi}^{\alpha\,\Delta\tau_1}\alpha\Delta\tau_1 + C_{T,\phi}^{\Delta\tau_1^2}\Delta\tau_1^2 \\ &\quad + C_{T,\phi}^{\Delta\tau_1}\Delta\tau_1\Big) + \overline{q}C_T^{\Delta\tau_1}\Delta\tau_1\Big] \\ &\quad \times \sin\alpha\Big/(mV) + \Delta L/(mV) \\ &\quad + \overline{q}S\Big(C_L^{\Delta\tau_1}\Delta\tau_1 + C_L^{\Delta\tau_2}\Delta\tau_2\Big)\Big/(mV), \\ g_\gamma(\alpha) &= \overline{q}S\,C_L^{\alpha}\Big/(mV) \\ &\quad + \overline{q}\phi\sin\alpha(C_{T,\phi}^{\alpha} + C_{T,\phi}^{\alpha M_\infty^{-2}}M_\infty^{-2}) \\ &\quad \Big/(mV) + \overline{q}\sin\alpha C_T^{\alpha}/(mV),\end{aligned} \tag{20}$$

$$\begin{aligned}f_\alpha(\gamma,\alpha,Q) &= f_{\alpha 0}(\gamma,\alpha,Q) \\ &\quad + \Delta f_\alpha(\gamma,\alpha,Q) - g_\alpha(\alpha)\alpha, \\ f_{\alpha 0}(\gamma,\alpha,Q) &= -f_{\gamma 0}(\gamma,\alpha), \Delta f_\alpha(\gamma,\alpha,Q) \\ &= -\Delta f_\gamma(\gamma,\alpha), g_\alpha = 1, T_1 \\ &= \overline{q}(\phi C_{T,\phi,1} + C_{T,1}), \\ f_Q(\gamma,\alpha,Q) &= f_{Q0}(\gamma,\alpha,Q) \\ &\quad + \Delta f_Q(\gamma,\alpha,Q), f_{Q0}(\gamma,\alpha,Q) \\ &= \Big[z_T T_1 + \overline{q}S\overline{c}(C_M^{\alpha}\alpha + C_M^{0})\Big]\Big/ I_{yy}, \\ \Delta f_Q(\gamma,\alpha,Q) &= \Big[z_T\Delta T + \overline{q}S\overline{c}\Big(\Delta C_M + C_M^{\Delta\tau_1}\Delta\tau_1 \\ &\quad + C_M^{\Delta\tau_2}\Delta\tau_2\Big)\Big]\Big/ I_{yy}, \\ g_Q(\gamma,\alpha,Q) &= \overline{q}S\overline{c}(C_M^{\delta_e} + C_M^{\delta_c}k_{ec0})\Big/ I_{yy}.\end{aligned}$$

In Eqs. (16)–(19), functions f_V, f_γ, f_α, f_Q, g_V, g_γ, and g_Q are unknown. The respective control inputs for velocity and altitude subsystems are designed in Sect. 3.

Remark 1 In [15,28,29], the COM is derived based on the assumption that the canard deflection δ_c is a function of the elevator deflection δ_e so that $\delta_c = k_{ec}\delta_e$,

Table 1 Admissible ranges of states, inputs, dynamic pressure, and Mach number [24,30,50]

State	Min.value	Max.value	State	Min.value	Max.value
h(ft)	70,000	1,35,000	ϕ	0.1	1.5
V(ft/s)	7,500	11,000	δ_c(rad)	−0.4712	0.4712
γ(rad)	−0.0524	0.0524	δ_e(rad)	−0.3491	0.3491
α(rad)	−0.0873	0.1746	$\overline{q}$(psf)	200	2,200
Q(rad/s)	−0.1746	0.1746	Ma	7	12

where $k_{ec} = -C_L^{\delta_e} / C_L^{\delta_c}$. Herein we consider k_{ec} uncertainty. It is more reasonable from the practical viewpoint.

2.2 Control objective

There are four inputs in (1)–(5) and they are the diffuser area ratio A_d (in this research, the diffuser area ratio A_d is fitted as $A_d = 1$), canard deflection δ_c, fuel equivalence ratio ϕ, and elevator deflection δ_e. The output to be controlled is selected as $y = [V, h]^T$. The control objective is to design the control inputs fuel equivalence ratio ϕ and elevator deflection δ_e for the COM such that the altitude and velocity follow their respective reference commands even in the presence of uncertain aerodynamic parameters and input constraints. Here, we only consider the cruise phase and leave out the ascent phase and the reentry phase. According to references [24,30,50], during the cruise phase, states, inputs, and reference trajectories are assumed to be within admissible ranges as given in Table 1.

In practice, due to physical limitations, the outputs of the actuator are constrained. One common example of such constraints is actuator saturation, which imposes a limitation on the magnitude of achievable control input [56,57]. Input constraints studied herein include the constraints on fuel equivalence ratio and elevator deflection. The constraint on fuel equivalence ratio is imposed by the very nature of the propulsion system, which is required to maintain the conditions that sustain scramjet operation [31]. If the constraint is exceeded, the thermal choking will occur, which is critical because it could lead to engine unstart that could jeopardize the mission, the vehicle, and its contents [58]. The constraint on elevator deflection is mainly imposed by the limits on the control surface displacement. The above input constraints can be expressed as

$$\phi = \begin{cases} \phi_{\max}, & \phi_c \geq \phi_{\max} \\ \phi_c, & \phi_{\min} < \phi_c < \phi_{\max} \\ \phi_{\min}, & \phi_c \leq \phi_{\min} \end{cases}, \tag{21}$$

$$\delta_e = \begin{cases} \delta_{e\max}, & \delta_{ec} \geq \delta_{e\max} \\ \delta_{ec}, & \delta_{e\min} < \delta_{ec} < \delta_{e\max} \\ \delta_{e\min}, & \delta_{ec} \leq \delta_{e\min} \end{cases}, \tag{22}$$

where ϕ_c and δ_{ec} are the desired control inputs to be designed in the subsequent section. $\phi_{\min}$ and $\phi_{\max}$ are the minimum value and maximum value of the fuel equivalence ratio, respectively. $\delta_{e\min}$ and $\delta_{e\max}$ are the minimum value and maximum value of the elevator deflection, respectively.

The velocity is controlled by fuel equivalence ratio which is designed by combining RBFNN and robust adaptive control method. The altitude is controlled by elevator deflection through the stable tracking of FPA reference command. The elevator deflection is developed by combining RBFNN and robust adaptive DSC. The FPA reference command γ_d is derived from altitude reference command h_d which is generated by the filtered step signals. FPA is controlled through AOA (which is regarded as a virtual control input and denoted as $\overline{\alpha}_d$). AOA is controlled through pitch rate (which is regarded as a virtual control input and denoted as $\overline{Q}_d$). Pitch rate is controlled by the elevator deflection δ_e. The design procedure is discussed in the succeeding section.

3 Controller design

As shown in the preceding section, every subsystem is controlled separately by the available input. It is obvious that the equations (17)–(19) possess pure-feedback formulation which makes the backstepping technique applicable. Backstepping control is proposed by Kokotovic [59,60]. It is a systematic and methodical approach. The principle idea is that the complex system is firstly decomposed into the lower dimension subsystems, and then the Lyapunov functions and the intermediate virtual control inputs are recursively designed for every subsystem. Recursive design procedure proceeds iteratively until the actual control input

is obtained. It is noted that the backstepping approach suffers from the "explosion of terms" problem induced by the repeated analytic derivative of the virtual control input. This problem grows drastically as the system order increases. To eliminate it, DSC approach is presented for nonlinear strict or pure-feedback system [61–64]. The synthetic input at each step of backstepping procedure is filtered by a first-order filter. Here, robust adaptive DSC and RBFNN are integrated to design control inputs for the velocity and altitude subsystems. In order to deal with input constraints, additional systems are developed to analyze the effect of input constraints. The states of them are utilized at the level of control design and stability analysis. Moreover, unknown functions are approximated by RBFNNs. It should be pointed out that all rigid body states are assumed to be measured.

3.1 Radial basis function neural network (RBFNN)

Universal function approximation approaches such as neural networks (NNs), fuzzy logic systems (FLS), polynomials, and splines have been widely employed in control design of nonlinear systems owing to their approximation capabilities under certain conditions. There are many kinds of NN such as RBFNN and wavelet neural network (WNN). In the paper, RBFNN is introduced to cope with unknown functions for its inherent properties in approximating any smooth nonlinear functions within arbitrary accuracy. The RBFNN is briefly introduced in this subsection and the detail is referred from [65–67].

The RBFNN takes the form $w^T\xi(x)$, where $w \in R^N$ is the weight vector (N is the NN node number) and $\xi(x) : R^n \to R^N$ is a vector function of input $x, \xi(x) = [\rho_1(x), \cdots \rho_N(x)]^T$, with $\rho_i(x)$ called a basis function and is chosen as the commonly used Gaussian function, which has the form

$$\rho_i(x) = \frac{1}{\sqrt{2\pi}\sigma}\exp\left(-\frac{\|\mathrm{x}-\zeta_\mathrm{i}\|^2}{2\sigma^2}\right), \mathrm{i} = 1, \ldots \mathrm{N}. \tag{23}$$

Here, $\zeta_i \in R^p$ is the center of the *ith* basis function and σ is a positive real number representing the width of basis functions.

Given a continuous real-valued function $F(\cdot) : R^n \to R$ on a compact set $\Omega_x \subset R^n$, and any $\delta_m > 0$, there exists an ideal weight vector $w^* \in R^N$ such that RBFNN $w^{*T}\xi(x)$ can approximate the given function $F(\cdot)$ with error δ^*, and the approximate formulation is

$$F(x) = w^{*T}\xi(x) + \delta^*, \tag{24}$$

here $|\delta^*| \le \delta_m$ and δ^* is the network reconstruction error. The formulation is

$$\delta^* = F(x) - w^{*T}\xi(x), \tag{25}$$

the ideal weight vector w^* is an artificial quantity required only for analytic purpose. It is defined as the value of w that minimizes $|\delta^*|$, i.e.,

$$w^* = \arg\min_{w\in R^n}\left\{\sup_{\xi\in\Omega_\xi}\left|F(x) - w^T\xi(x)\right|\right\}, \tag{26}$$

it is clear that w^* is usually unknown and needs to be estimated.

3.2 Controller design for velocity subsystem

In this subsection, the control input is designed for the velocity subsystem where input constraint (21) and aerodynamic uncertainty are taken into consideration.

The dynamic equation (16) can be expressed as

$$\dot{V} = F_V(V) + \phi, \tag{27}$$

where $F_V(V) = f_V + g_V\phi - \phi$ is an unknown function. We only need one RBFNN to estimate the unknown function. If the controller is designed based on (16), two RBFNNs are needed to estimate unknown functions f_V and g_V.

The velocity tracking error is defined as $z_V = V - V_d$, where V_d is the velocity reference command. The velocity tracking error dynamic is

$$\dot{z}_V = F_V(V) + \phi - \dot{V}_d. \tag{28}$$

Note that $F_V(V)$ is an unknown function. Based on RBFNN(24), the approximate formulation of $F_V(V)$ is

$$F_V(V) = w_V^{*T}\xi_V(V) + \delta_V^*, \left|\delta_V^*\right| \le \delta_m. \tag{29}$$

Since w_V^* needs to be estimated online, the representation $\hat{w}_V^*$ denotes the estimation which is updated by adaptive law. For the simplicity of writing, the function arguments are removed in brief.

In order to systematically account for the constraints during the controller design procedure of FAHV, we will henceforth benefit from the method presented in [68]. Inspired by the work in that literature, an additional system is constructed to analyze the impact of

the input constraint (21), and the state of which is used for controller design. The additional system has the following formulation

$$\dot{\sigma}_\phi = \begin{cases} -k_{\sigma_\phi}\sigma_\phi - (|z_V \Delta\phi| \\ \quad +0.5\Delta\phi^2)/\sigma_\phi - \Delta\phi, & |\sigma_\phi| \geq \psi_\phi, \\ 0 & |\sigma_\phi| < \psi_\phi \end{cases} \tag{30}$$

where σ_ϕ is the state of the additional system. ψ_ϕ is a small positive design parameter and should be chosen as an appropriate value according to the requirement of the tracking performance. $\Delta\phi = \phi - \phi_c$ is the error between the actual control input ϕ provided by the actuator and the desired control input ϕ_c designed by the following control law.

Remark 2 From the backgrounds of FAHV, fuel equivalence ratio must be positive, thus its constraint is asymmetric, i.e., $\phi_{\max} \neq -\phi_{\min}$. However, the constraint of elevator deflection can be asymmetric or symmetric. The method adopted here can tackle asymmetric and symmetric input constraints simultaneously. Moreover, from the stability analysis, we can obtain that the control inputs ϕ and δ_e produced by the designed control inputs ϕ_c and δ_{ec} can ensure the stability of the closed-loop system.

The desired control input of the velocity subsystem is designed as

$$\phi_c = -k_V(z_V - \sigma_\phi) + \dot{V}_d - \frac{z_V \mu_\phi(z_V)}{\xi_\phi^2 + z_V^2} - \hat{w}_V^{*T}\xi_V, \tag{31}$$

with

$$\mu_\phi(z_V) = 0.5k_V^2 z_V^2, \dot{\xi}_\phi = \begin{cases} -k_{\xi_\phi}\xi_\phi - \frac{\mu_\phi(z_V)\xi_\phi}{\xi_\phi^2 + z_V^2}, & |z_V| \geq \psi_V \\ 0, & |z_V| < \psi_V \end{cases}. \tag{32}$$

Here, $\psi_V > 0$ and it should also be chosen as an appropriate value according to the requirement of the tracking performance. $\hat{w}^*$ is the estimation value of w^*. The adaptive law for $\hat{w}^*$ is as follows

$$\dot{\hat{w}}_V^* = \Gamma_V(\xi_V z_V - b_V \hat{w}_V^*), \tag{33}$$

where $k_V, b_V > 0$, and Γ_V is a positive definite diagonal matrix.

Taking the velocity tracking error and estimation error of $\hat{w}^*$ into consideration, the Lyapunov function is constructed as

$$Y_V = \frac{1}{2}z_V^2 + \frac{1}{2}\tilde{w}_V^{*T}\Gamma_V^{-1}\tilde{w}_V^* + \frac{1}{2}\xi_\phi^2 + \frac{1}{2}\sigma_\phi^2, \tag{34}$$

where $\tilde{w}_V^* = \hat{w}_V^* - w_V^*$ is the estimation error of w_V^*.

Using the derivative of Y_V with respect to time, $\dot{Y}_V = z_V \dot{z}_V + \tilde{w}_V^* \Gamma_V^{-1} \dot{\hat{w}}_V^* + \xi_\phi \dot{\xi}_\phi + \sigma_\phi \dot{\sigma}_\phi$. Based on (30)–(33), we have

$$\begin{aligned} \dot{Y}_V = & -k_V z_V^2 - k_{\sigma_\phi}\sigma_\phi^2 - k_{\xi_\phi}\xi_\phi^2 + k_V \sigma_\phi z_V + z_V \Delta\phi \\ & - |z_V \Delta\phi| - \frac{1}{2}\Delta\phi^2 - \sigma_\phi \Delta\phi \\ & - \frac{z_V^2 \mu_\phi(z_V)}{\xi_\phi^2 + z_V^2} - \frac{\mu_\phi(z_V)\xi_\phi^2}{\xi_\phi^2 + z_V^2} - z_V \hat{w}_V^{*T}\xi_V \\ & + z_V w_V^{*T}\xi_V + z_V \delta_V^* + z_V \tilde{w}_V^{*T}\xi_V - b_V \tilde{w}_V^{*T}\hat{w}_V^*, \end{aligned} \tag{35}$$

since

$$\begin{aligned} -\frac{z_V^2 \mu_\phi(z_V)}{\xi_\phi^2 + z_V^2} = & -\mu_\phi(z_V) \\ & + \frac{\mu_\phi(z_V)\xi_\phi^2}{\xi_\phi^2 + z_V^2}, z_V \Delta\phi - |z_V \Delta\phi| \leq 0, \end{aligned}$$

$$\begin{aligned} \mu_\phi(z_V) &= \frac{1}{2}k_V^2 z_V^2, k_V \sigma_\phi z_V - \sigma_\phi \Delta\phi \\ &\leq \frac{1}{2}k_V^2 z_V^2 + \sigma_\phi^2 + \frac{1}{2}\Delta\phi^2, \\ &\quad - z_V \hat{w}_V^{*T}\xi_V + z_V w_V^{*T}\xi_V + z_V \delta_V^* \\ &\quad + z_V \tilde{w}_V^{*T}\xi_V - b_V \tilde{w}_V^{*T}\hat{w}_V^* \\ &= z_V \delta_V^* - b_V \tilde{w}_V^{*T}\hat{w}_V^* \\ &\leq z_V^2 + \frac{\delta_m}{4} - \frac{b_V}{2}\left\|\tilde{w}_V^*\right\|^2 + \frac{b_V}{2}\left\|w_V^*\right\|^2, \end{aligned}$$

equality (35) becomes

$$\begin{aligned} \dot{Y}_V \leq & -(k_V - 1)z_V^2 - (k_{\sigma_\phi} - 1)\sigma_\phi^2 - k_{\xi_\phi}\xi_\phi^2 \\ & - \frac{b_V}{2}\left\|\tilde{w}_V^*\right\|^2 + \frac{\delta_m}{4} + \frac{b_V}{2}\left\|w_V^*\right\|^2, \end{aligned} \tag{36}$$

where $k_V, k_{\sigma_\phi} > 1$ are the parameters to be designed.

Remark 3 The constraint of fuel equivalence ratio in control law (31) is shown through the role of the term $k_V \sigma_\phi$ based on the input constraint block (21) as follows.

If $|\sigma_\phi| \geq \psi_\phi > 0$, there is input saturation: (a) If $\phi_c \geq \phi_{\max}$, the term $k_V \sigma_\phi$ keeps changing to decrease the designed input ϕ_c until $\phi_c = \phi_{\max}$. (b) If$\phi_c \leq \phi_{\min}$, the term $k_V \sigma_\phi$ keeps changing to increase the designed input ϕ_c until $\phi_c = \phi_{\min}$. Thus, $\phi = \phi_{\max}$ or $\phi = \phi_{\min}$.

If $|\sigma_\phi| < \psi_\phi, \dot{\sigma}_\phi = 0$, there is no input saturation, $\Delta\phi = 0$. The term $k_V \sigma_\phi$ makes the designed input satisfy $\phi_{\min} \leq \phi_c \leq \phi_{\max}$. Hence, $\phi = \phi_c$.

3.3 Controller design for altitude subsystem

The altitude subsystem comprised dynamic equations of altitude, FPA, AOA, and pitch rate. Given an altitude reference command h_d, the tracking error is defined as $z_h = h - h_d$. Since the paper only considers the cruise phase, without loss of generality, the FPA is generally small. Using the approximation $\sin\gamma \approx \gamma$ which is valid for the small value of FPA as shown in Table 1, the altitude tracking error dynamic is $\dot{z}_h \approx V\gamma - \dot{h}_d$ [4,28–30]. The altitude is controlled via the tracking of FPA reference command γ_d which is derived as follows

$$\gamma_d = [-k_h(h - h_d) + \dot{h}_d]/V, \tag{37}$$

where $k_h > 0$ is the parameter to be designed.

From aerospace engineering backgrounds of hypersonic vehicle, there is a time scale separation between altitude and FPA. Altitude dynamic can be regarded as the "slow" time scale dynamic, while FPA dynamic can be considered as the "fast" time scale dynamic. The transient dynamics of the fast-state FPA occur so quickly that they have negligible effect on the slow states. The "fast" time scale controller attempts to maintain the FPA close to its reference command γ_d actual value in the "slow" time scale dynamic. That is to say, in the altitude dynamic $\dot{h} \approx V\gamma$, the relation $\gamma_d = \gamma$ holds after a very short time, so the dynamic of altitude tracking error satisfies $\dot{z}_h = V\gamma_d - \dot{h}_d$. Substituting (37) into it yields [6,28]

$$\dot{z}_h = -k_h z_h. \tag{38}$$

Thus, if the flight path angle is controlled to follow the reference command γ_d, the altitude can achieve stable tracking of its reference command. In what follows, we focus on designing the controller to achieve stable tracking of FPA reference command.

In Eqs. (17)–(19), $f_\gamma(\gamma,\alpha)$, $g_\gamma(\gamma,\alpha)$, $f_\alpha(\gamma,\alpha,Q)$, $f_Q(\gamma,\alpha,Q)$, and $g_Q(\gamma,\alpha,Q)$ are unknown. Five RBFNNs are needed to approximate them. Motivated by the research in [62], we can rewrite the Eqs. (17)–(19) as the following formulation

$$\dot{\gamma} = F_\gamma(\gamma,\alpha) + \alpha, \tag{39}$$

$$\dot{\alpha} = F_\alpha(\gamma,\alpha,Q) + Q, \tag{40}$$

$$\dot{Q} = F_Q(\gamma,\alpha,Q) + \delta_e, \tag{41}$$

where the unknown functions $F_\gamma(\gamma,\alpha) = f_\gamma(\gamma,\alpha) + g_\gamma(\alpha)\alpha - \alpha$, $F_\alpha(\gamma,\alpha,Q) = -F_\gamma(\gamma,\alpha) + \alpha$, and $F_Q(\gamma,\alpha,Q) = f_Q(\gamma,\alpha,Q) + G_Q\delta_e - \delta_e$ are approximated by three RBFNNs.

Using RBFNN (24) to carry out the approximation, the above unknown functions can be expressed as

$$F_\gamma(\gamma,\alpha) = w_\gamma^{*T}\xi_\gamma(x) + \delta_\gamma^*,\ \left|\delta_\gamma^*\right| \le \delta_m, \tag{42}$$

$$F_\alpha(\gamma,\alpha,Q) = w_\alpha^{*T}\xi_\alpha(x) + \delta_\alpha^*,\ \left|\delta_\alpha^*\right| \le \delta_m, \tag{43}$$

$$F_Q(\gamma,\alpha,Q) = w_Q^{*T}\xi_Q(x) + \delta_Q^*,\ \left|\delta_Q^*\right| \le \delta_m, \tag{44}$$

the ideal weight vectors w_γ^*, w_α^*, and w_Q^* are unknown and need to be estimated. Furthermore, adaptive laws are designed to update their estimations. In order to reduce the computational burden, the MLP technique proposed in [69,70] is employed to estimate the maximum norm of the ideal weight vectors w_γ^*, w_α^*, and w_Q^* rather than their elements, so only one parameter needs to be updated online. This parameter is defined as

$$\varphi = \max\left\{\left\|w_l^*\right\|^2,\ \ l = \gamma,\alpha,Q\right\}. \tag{45}$$

Here, φ needs to be estimated because w_l^* is unknown. The estimation is denoted as $\hat{\varphi}$ with $\hat{\varphi}(t) \ge 0$.

Remark 4 In the paper, only one parameter φ needs to be estimated online by the MLP technique during RBFNN-based controller design procedure of altitude subsystem. However, a lot of parameters need to be estimated in the NN-approximation-based control scheme for AHV, such as [45–48], which requires large computational burden.

In what follows, the controller is designed for (39)–(41) via synthesizing RBFNN and DSC technique. Similar to the backstepping control approach, the design consists of three steps. In the first two steps, the virtual control inputs (here, states AOA and pitch rate are regarded as virtual control inputs) are developed. The actual control input is presented in the last step. The altitude is controlled through the tracking of FPA reference command γ_d given in (37). Thus, the controller design begins from Eq. (39).

Step 1 We define the first error surface (FPA tracking error) as $S_\gamma = \gamma - \gamma_d$, the time derivative along (39) is

$$\dot{S}_\gamma = F_\gamma(\gamma,\alpha) + \alpha - \dot{\gamma}_d. \tag{46}$$

The virtual control input is designed as

$$\overline{\alpha}_d = -\left(k_\gamma + \frac{1}{2a_\gamma^2} + \frac{a_\gamma^2}{2}\right)S_\gamma - \frac{a_\gamma^2}{2}S_\gamma\hat{\varphi}\xi_\gamma^T\xi_\gamma + \dot{\gamma}_d, \tag{47}$$

where $k_\gamma, a_\gamma > 0$ are the parameters to be designed.

With the tracking error and RBFNN estimation error, the Lyapunov function is constructed as

$$Y_\gamma = \frac{1}{2}S_\gamma^2 + \frac{1}{2\lambda}\tilde{\varphi}^2, \tag{48}$$

where $\tilde{\varphi} = \hat{\varphi} - \varphi$ and λ is a positive parameter to be designed.

Based on (39), the time derivative of Y_γ is

$$\begin{aligned}\dot{Y}_\gamma &= S_\gamma F_\gamma(\gamma,\alpha) + S_\gamma(\alpha - \overline{\alpha}_d) \\ &\quad + S_\gamma\overline{\alpha}_d - S_\gamma\dot{\gamma}_d + \frac{1}{\lambda}\tilde{\varphi}\dot{\hat{\varphi}},\end{aligned} \tag{49}$$

using (42) and Young's inequality, the first term on the right-hand side satisfies

$$\begin{aligned}&S_\gamma F_\gamma(\gamma,\alpha) = S_\gamma(w_\gamma^{*T}\xi_\gamma(x) + \delta_\gamma^*) \\ &\le \frac{a_\gamma^2 S_\gamma^2}{2}w_\gamma^{*T}w_\gamma^*\xi_\gamma^T\xi_\gamma + \frac{1}{2a_\gamma^2} + \frac{a_\gamma^2 S_\gamma^2}{2} \\ &\quad + \frac{\delta_m^2}{2a_\gamma^2} \le \frac{a_\gamma^2 S_\gamma^2}{2}\varphi\xi_\gamma^T\xi_\gamma + \frac{1}{2a_\gamma^2} + \frac{a_\gamma^2 S_\gamma^2}{2} + \frac{\delta_m^2}{2a_\gamma^2},\end{aligned} \tag{50}$$

submitting (47) and (50) into (49) yields

$$\begin{aligned}\dot{Y}_\gamma &\le S_\gamma(\alpha - \overline{\alpha}_d) + S_\gamma\overline{\alpha}_d - S_\gamma\dot{\gamma}_d + \frac{a_\gamma^2 S_\gamma^2}{2}\varphi\xi_\gamma^T\xi_\gamma \\ &\quad + \frac{1}{2a_\gamma^2} + \frac{a_\gamma^2 S_\gamma^2}{2} + \frac{\delta_m^2}{2a_\gamma^2} + 1/\lambda\tilde{\varphi}\dot{\hat{\varphi}} \\ &\le S_\gamma(\alpha - \overline{\alpha}_d) - k_\gamma S_\gamma^2 - \frac{S_\gamma^2}{2a_\gamma^2} \\ &\quad + \frac{1}{\lambda}\tilde{\varphi}\left(\dot{\hat{\varphi}} - \frac{\lambda a_\gamma^2 S_\gamma^2}{2}\xi_\gamma^T\xi_\gamma\right) + \frac{1}{2a_\gamma^2} + \frac{\delta_m^2}{2a_\gamma^2}.\end{aligned} \tag{51}$$

A new variable α_d is obtained by letting $\overline{\alpha}_d$ pass through the following first-order filter

$$\tau_\alpha\dot{\alpha}_d + \alpha_d = \overline{\alpha}_d, \overline{\alpha}_d(0) = \alpha_d(0), \tag{52}$$

where $\tau_\alpha > 0$ is the time constant.

The filter estimation error is defined as

$$\chi_\alpha = \alpha_d - \overline{\alpha}_d. \tag{53}$$

Step 2 We define the second error surface as

$$S_\alpha = \alpha - \alpha_d, \tag{54}$$

from (53) and (54), (51) becomes

$$\begin{aligned}\dot{Y}_\gamma &\le S_\gamma\chi_\alpha + S_\gamma S_\alpha - k_\gamma S_\gamma^2 \\ &\quad - \frac{S_\gamma^2}{2a_\gamma^2} + \frac{1}{\lambda}\tilde{\varphi}\left(\dot{\hat{\varphi}} - \frac{\lambda a_\gamma^2 S_\gamma^2}{2}\xi_\gamma^T\xi_\gamma\right) \\ &\quad + \frac{1}{2a_\gamma^2} + \frac{\delta_m^2}{2a_\gamma^2},\end{aligned} \tag{55}$$

it should be pointed out that the coupling term $S_\gamma S_\alpha$ will be cancelled in the subsequent step.

The time derivative of (54) along with (40) is

$$\dot{S}_\alpha = F_\alpha(\gamma,\alpha,Q) + Q - \dot{\alpha}_d. \tag{56}$$

The virtual control input is developed as

$$\begin{aligned}\overline{Q}_d &= -\left(k_\alpha + \frac{1}{2a_\alpha^2} + \frac{a_\alpha^2}{2}\right)S_\alpha \\ &\quad - \frac{a_\alpha^2}{2}S_\alpha\hat{\varphi}\xi_\alpha^T\xi_\alpha + \dot{\alpha}_d - S_\gamma,\end{aligned} \tag{57}$$

where k_α and a_α are positive parameters to be designed, and the last term on the right-hand side is used to cancel the residual coupling term $S_\gamma S_\alpha$ in(55).

Taking the error surface into account, the following Lyapunov function is constructed

$$Y_\alpha = \frac{1}{2}S_\alpha^2. \tag{58}$$

The time derivative of Y_α yields

$$\begin{aligned}\dot{Y}_\alpha &= S_\alpha F_\alpha(\gamma,\alpha,Q) + S_\alpha(Q - \overline{Q}_d) \\ &\quad + S_\alpha\overline{Q}_d - S_\alpha\dot{\alpha}_d.\end{aligned} \tag{59}$$

Based on (43) and Young inequality, the first term on the right-hand side satisfies

$$\begin{aligned}&S_\alpha F_\alpha(\gamma,\alpha,Q) \le \frac{a_\alpha^2 S_\alpha^2}{2}w_\alpha^{*T}w_\alpha^*\xi_\alpha^T\xi_\alpha + \frac{1}{2a_\alpha^2} + \frac{a_\alpha^2 S_\alpha^2}{2} \\ &\quad + \frac{\delta_m^2}{2a_\alpha^2} \le \frac{a_\alpha^2 S_\alpha^2}{2}\varphi\xi_\alpha^T\xi_\alpha + \frac{1}{2a_\alpha^2} + \frac{a_\alpha^2 S_\alpha^2}{2} + \frac{\delta_m^2}{2a_\alpha^2},\end{aligned} \tag{60}$$

where a_α is a positive parameter to be designed.

Submitting (57) and (60) into (59) yields

$$\begin{aligned}\dot{Y}_\alpha &\le S_\alpha(Q - \overline{Q}_d) + S_\alpha\overline{Q}_d - S_\alpha\dot{\alpha}_d \\ &\quad + \frac{a_\alpha^2 S_\alpha^2}{2}\varphi\xi_\alpha^T\xi_\alpha + \frac{1}{2a_\alpha^2} + \frac{a_\alpha^2 S_\alpha^2}{2} + \frac{\delta_m^2}{2a_\alpha^2} \\ &\le S_\alpha(Q - \overline{Q}_d) - k_\alpha S_\alpha^2 - \frac{1}{2a_\alpha^2}S_\alpha^2 \\ &\quad - \frac{a_\alpha^2 S_\alpha^2}{2}\tilde{\varphi}\xi_\alpha^T\xi_\alpha - S_\alpha S_\gamma + \frac{1}{2a_\alpha^2} + \frac{\delta_m^2}{2a_\alpha^2}.\end{aligned} \tag{61}$$

A new variable Q_d is obtained by letting $\overline{Q}_d$ pass through the following first-order filter

$$\tau_Q\dot{Q}_d + Q_d = \overline{Q}_d, \quad \overline{Q}_d(0) = Q_d(0), \tag{62}$$

where $\tau_Q > 0$ is a time constant.

The filter estimation error is defined as

$$\chi_Q = Q_d - \overline{Q}_d. \tag{63}$$

Step 3 We define the third error surface as

$$S_Q = Q - Q_d, \tag{64}$$

from (63) and (64), (61) becomes

$$\dot{Y}_\alpha \le S_\alpha(\chi_Q + S_Q) - k_\alpha S_\alpha^2 - \frac{1}{2a_\alpha^2}S_\alpha^2 - \frac{a_\alpha^2 S_\alpha^2}{2}\tilde{\varphi}\xi_\alpha^T\xi_\alpha - S_\alpha S_\gamma + \frac{1}{2a_\alpha^2} + \frac{\delta_m^2}{2a_\alpha^2}. \tag{65}$$

The time derivative of (64) along with (41) is

$$\dot{S}_Q = F_Q(\gamma, \alpha, Q) + \delta_e - \dot{Q}_d. \tag{66}$$

Considering the constraint on elevator deflection (22), an additional system is constructed to analyze the effect of constraint [68]

$$\dot{\sigma}_{\delta_e} = \begin{cases} -k_{\sigma_{\delta_e}}\sigma_{\delta_e} - (|S_Q\Delta\delta_e| \\ \quad + 0.5\Delta\delta_e^2)/\sigma_{\delta_e} - \Delta\delta_e, & |\sigma_{\delta_e}| \ge \psi_{\delta_e} \\ 0, & |\sigma_{\delta_e}| < \psi_{\delta_e} \end{cases}, \tag{67}$$

where σ_{δ_e} is the state of the additional system. ψ_{δ_e} is a small positive design parameter and should be chosen as an appropriate value according to the requirement of the tracking performance. $\Delta\delta_e = \delta_e - \delta_{ec}$ is the error between the actual control input δ_e provided by the actuator and the desired control input δ_{ec} designed by the control law.

The desired control input elevator deflection is designed as

$$\delta_{ec} = -\left(\frac{1}{2a_Q^2} + \frac{a_Q^2}{2}\right)S_Q - k_Q(S_Q - \sigma_{\delta_e}) + \dot{Q}_d - \frac{S_Q\mu_{\delta_e}(S_Q)}{\xi_{\delta_e}^2 + S_Q^2} - \frac{a_Q^2}{2}S_Q\hat{\varphi}\xi_Q^T\xi_Q - S_\alpha, \tag{68}$$

with

$$\mu_{\delta_e}(S_Q) = \frac{1}{2}k_Q^2 S_Q^2, \dot{\xi}_{\delta_e} = \begin{cases} -k_{\xi_{\delta_e}}\xi_{\delta_e} - \frac{\mu_{\delta_e}(S_Q)\xi_{\delta_e}}{\xi_\phi^2 + S_Q^2}, & |S_Q| \ge \psi_Q \\ 0, & |S_Q| < \psi_Q \end{cases}, \tag{69}$$

where ψ_ϕ is a small positive design parameter and should be chosen as an appropriate value according to the requirement of the tracking performance. In addition, $\hat{\varphi}$ is the estimation of φ.

The adaptive law for $\hat{\varphi}$ is given below

$$\dot{\hat{\varphi}} = \sum_{l=\gamma,\alpha,Q}\frac{\lambda a_l^2 S_l^2 \xi_l^T\xi_l}{2} - \vartheta\lambda\hat{\varphi}, \hat{\varphi}(0) \ge 0, \tag{70}$$

where $k_Q, k_{\xi_{\delta_e}}, \vartheta > 0$ are parameters to be designed.

Remark 5 The constraint of fuel equivalence ratio in control law (68) is shown through the role of the term $k_Q\sigma_{\delta_e}$ based on the input constraint block (22).

If $|\sigma_{\delta_e}| \ge \psi_{\delta_e} > 0$, there is input saturation: (a) If$\delta_{ec} \ge \delta_{e\max}$, the term $k_Q\sigma_{\delta_e}$ keeps changing to make the designed input δ_{ec} decrease until $\delta_{ec} = \delta_{e\max}$. (b) If $\delta_{ec} \le \delta_{e\min}$, the term $k_Q\sigma_{\delta_e}$ keeps changing to let the designed input δ_{ec} increase until $\delta_{ec} = \delta_{e\min}$. Thus, $\delta_e = \delta_{e\min}$ or $\delta_e = \delta_{e\max}$.

If $|\sigma_{\delta_e}| < \psi_{\delta_e}$, $\dot{\sigma}_{\delta_e} = 0$, there is no input saturation, $\Delta\delta_e = 0$. The term $k_Q\sigma_{\delta_e}$ makes the designed input δ_{ec} satisfy $\delta_{e\min} \le \delta_{ec} \le \delta_{e\max}$, so $\delta_e = \delta_{ec}$.

Considering the surface error and additional system, the Lyapunov function is constructed as

$$Y_Q = \frac{1}{2}S_Q^2 + \frac{1}{2}\xi_{\delta_e}^2 + \frac{1}{2}\sigma_{\delta_c}^2, \tag{71}$$

the time derivative yields

$$\dot{Y}_Q = S_Q(F_Q(\gamma, \alpha, Q) + \delta_{ec} + \Delta\delta_e - \dot{Q}_d) + \xi_{\delta_e}\dot{\xi}_{\delta_e} + \sigma_{\delta_e}\dot{\sigma}_{\delta_e}, \tag{72}$$

using (44) and Young's inequality, we have

$$\begin{aligned} S_Q F_Q(\gamma, \alpha, Q) &\le \frac{a_Q^2 S_Q^2}{2}w_Q^{*T}w_Q^*\xi_Q^T\xi_Q + \frac{1}{2a_Q^2} + \frac{a_Q^2 S_Q^2}{2} + \frac{\delta_m^2}{2a_Q^2} \\ &\le \frac{a_Q^2 S_Q^2}{2}\varphi\xi_Q^T\xi_Q + \frac{1}{2a_Q^2} + \frac{a_Q^2 S_Q^2}{2} + \frac{\delta_m^2}{2a_Q^2}, \end{aligned} \tag{73}$$

where a_Q is a positive parameter to be designed.

Submitting (68) and (73) into (72) yields

$$\begin{aligned} \dot{Y}_Q &\le S_Q\delta_{ec} + S_Q\Delta\delta_e - S_Q\dot{Q}_d + \frac{a_Q^2 S_Q^2}{2}\varphi\xi_Q^T\xi_Q + \frac{1}{2a_Q^2} + \frac{a_Q^2 S_Q^2}{2} + \frac{\delta_m^2}{2a_Q^2} + \xi_{\delta_e}\dot{\xi}_{\delta_e} + \sigma_{\delta_e}\dot{\sigma}_{\delta_e} \\ &\le -k_Q S_Q^2 - \frac{1}{2a_Q^2}S_Q^2 - \frac{a_Q^2 S_Q^2}{2}\tilde{\varphi}\xi_Q^T\xi_Q \end{aligned}$$

$$-S_\alpha S_Q + \frac{1}{2a_Q^2} + \frac{\delta_m^2}{2a_Q^2} \underbrace{-\frac{S_Q^2 \mu_{\delta_e}(S_Q)}{\xi_{\delta_e}^2 + S_Q^2} + k_Q \sigma_{\delta_e} S_Q + S_Q \Delta\delta_e + \xi_{\delta_e}\dot{\xi}_{\delta_e} + \sigma_{\delta_e}\dot{\sigma}_{\delta_e}}_{:=A}, \tag{74}$$

from (67) and (69), the term A on the right-hand side of (74) satisfies

$$\begin{aligned} A = & -\frac{S_Q^2 \mu_{\delta_e}(S_Q)}{\xi_{\delta_e}^2 + S_Q^2} + k_Q \sigma_{\delta_e} S_Q + S_Q \Delta\delta_e \\ & - k_{\sigma_{\delta_e}} \sigma_{\delta_e}^2 - k_{\xi_{\delta_e}} \xi_{\delta_e}^2 \\ & - \frac{\mu_{\delta_e}(S_Q)\xi_{\delta_e}^2}{\xi_{\delta_e}^2 + S_Q^2} - (\left|S_Q \Delta\delta_e\right| + 0.5\Delta\delta_e^2) \\ & - \sigma_{\delta_e}\Delta\delta_e, \end{aligned} \tag{75}$$

since $-\frac{S_Q^2 \mu_{\delta_e}(S_Q)}{\xi_{\delta_e}^2 + S_Q^2} = -\mu_{\delta_e}(S_Q) + \frac{\mu_{\delta_e}(S_Q)\xi_{\delta_e}^2}{\xi_{\delta_e}^2 + S_Q^2}$, $\mu_{\delta_e}(S_Q) = 0.5k_Q^2 S_Q^2$, $S_Q\Delta\delta_e - \left|S_Q\Delta\delta_e\right| \le 0$, and $k_Q\sigma_{\delta_e}S_Q - \sigma_{\delta_e}\Delta\delta_e \le 0.5k_Q^2 S_Q^2 + \sigma_{\delta_e}^2 + 0.5\Delta\delta_e^2$, (75) satisfies

$$A \le -(k_{\sigma_{\delta_e}} - 1)\sigma_{\delta_e}^2 - k_{\xi_{\delta_e}}\xi_{\delta_e}^2, \tag{76}$$

submitting (76) into (74), the following inequality holds

$$\begin{aligned} \dot{Y}_Q \le & -k_Q S_Q^2 - \frac{1}{2a_Q^2} S_Q^2 - (k_{\sigma_{\delta_e}} - 1)\sigma_{\delta_e}^2 \\ & - k_{\xi_{\delta_e}}\xi_{\delta_e}^2 - \frac{a_Q^2 S_Q^2}{2}\tilde{\varphi}\xi_Q^T\xi_Q \\ & - S_\alpha S_Q + \frac{1}{2a_Q^2} + \frac{\delta_m^2}{2a_Q^2}. \end{aligned} \tag{77}$$

Remark 6 This paper contains the following different aspects compared to the existing results [6,45,46,48] which investigate the controller design of AHV based on DSC.

(a) The robustness of the designed scheme in [46] is evaluated through different fuel levels. However, the robustness of the scheme developed herein is shown through aerodynamic uncertainty.
(b) Compared to the research in [6,45,48], we transform the altitude subsystem into the formulation (39)–(41) which does not need to estimate their input coefficient functions using RBFNNs. Moreover, MLP technique is used to estimate the maximum norm of the ideal weight vectors of RBFNN instead of their elements. Through combining DSC and MLP techniques, the control strategy proposed in this paper can simultaneously solve problems of explosion of learning parameters and "explosion of terms" which leads to a much simpler controller with less computational load.

4 Stability analysis

In this section, the stability analysis for the rigid body system is given on the basis of the former section. We can obtain that the respective tracking errors of velocity and altitude converge to the arbitrarily small neighborhood around zero by appropriately choosing the design parameters. In addition, stability of flexible states will be evaluated through simulation in Sect. 5.

From (52)–(53) and (62)–(63), we have

$$\dot{\alpha}_d = -\frac{\chi_\alpha}{\tau_\alpha}, \quad \dot{Q}_d = -\frac{\chi_Q}{\tau_Q}, \tag{78}$$

then the filter estimation error dynamics are

$$\dot{\chi}_\alpha = -\frac{\chi_\alpha}{\tau_\alpha} - \dot{\bar{\alpha}}_d, \dot{\chi}_Q = -\frac{\chi_Q}{\tau_Q} - \dot{\bar{Q}}_d. \tag{79}$$

From (47) and (57), the following can be obtained

$$\begin{aligned} \dot{\bar{\alpha}}_d = & -\left(k_\gamma + \frac{1}{2a_\gamma^2} + \frac{a_\gamma^2}{2}\right)\dot{S}_\gamma \\ & -\frac{a_\gamma^2}{2}\left(\dot{S}_\gamma\hat{\varphi}\xi_\gamma^T\xi_\gamma + S_\gamma\dot{\hat{\varphi}}\xi_\gamma^T\xi_\gamma\right) \\ & -\frac{a_\gamma^2}{2}S_\gamma\hat{\varphi}\left(\frac{\partial(\xi_\gamma^T\xi_\gamma)}{\partial\gamma}\dot{\gamma} + \frac{\partial(\xi_\gamma^T\xi_\gamma)}{\partial\alpha}\dot{\alpha}\right) + \ddot{\gamma}_d. \end{aligned} \tag{80}$$

$$\begin{aligned} \dot{\bar{Q}}_d = & -\left(k_\alpha + \frac{1}{2a_\alpha^2} + \frac{a_\alpha^2}{2}\right)\dot{S}_\alpha \\ & -\frac{a_\alpha^2}{2}\left(\dot{S}_\alpha\hat{\varphi}\xi_\alpha^T\xi_\alpha + S_\alpha\dot{\hat{\varphi}}\xi_\alpha^T\xi_\alpha\right) \\ & -\frac{a_\alpha^2}{2}S_\alpha\hat{\varphi}\left(\frac{\partial\dot{\xi}_\alpha^T\xi_\alpha}{\partial\gamma}\dot{\gamma} + \frac{\partial\dot{\xi}_\alpha^T\xi_\alpha}{\partial\alpha}\dot{\alpha}\right) + \ddot{\alpha}_d - \dot{S}_\alpha. \end{aligned} \tag{81}$$

The Lyapuonov function is chosen as

$$Y = Y_V + Y_h + Y_\gamma + Y_\alpha + Y_Q \ + \frac{1}{2}\chi_\alpha^2 + \frac{1}{2}\chi_Q^2. \tag{82}$$

Here $Y_h = \frac{1}{2}z_h^2$.

Using the derivative of (82) with respect to time,

$$\dot{Y} = \dot{Y}_V + \dot{Y}_h + \dot{Y}_\gamma + \dot{Y}_\alpha + \dot{Y}_Q + \chi_\alpha \dot{\chi}_\alpha + \chi_Q \dot{\chi}_Q. \tag{83}$$

From (36), (38), (55), (65), (70), and (77), it yields the following inequality

$$\begin{aligned}\dot{Y} \le & -(k_V - 1)z_V^2 - (k_{\sigma_\phi} - 1)\sigma_\phi^2 - k_{\xi_\phi}\xi_\phi^2 \\ & -\frac{b_V}{2}\left\|\tilde{w}_V^*\right\|^2 - k_h z_h^2 - k_\gamma S_\gamma^2 - \frac{1}{2a_\gamma^2}S_\gamma^2 \\ & - k_\alpha S_\alpha^2 - \frac{1}{2a_\alpha^2}S_\alpha^2 \quad - k_Q S_Q^2 \\ & -\frac{1}{2a_Q^2}S_Q^2 - (k_{\sigma_{\delta_e}} - 1)\sigma_{\delta_e}^2 \ - k_{\xi_{\delta_e}}\xi_{\delta_e}^2 \\ & + S_\gamma \chi_\alpha + S_\alpha \chi_Q - \vartheta\tilde{\varphi}\hat{\varphi} + \chi_\alpha \dot{\chi}_\alpha \\ & + \chi_Q \dot{\chi}_Q + \frac{1}{2a_\gamma^2} + \frac{\delta_m^2}{2a_\gamma^2} + \frac{1}{2a_\alpha^2} + \frac{\delta_m^2}{2a_\alpha^2} \\ & + \frac{1}{2a_Q^2} + \frac{\delta_m^2}{2a_Q^2} + \frac{\delta_m}{4} + \frac{b_V}{2}\left\|w_V^*\right\|^2, \end{aligned} \tag{84}$$

according to [62,63], (80) and (81) satisfy $\left|\dot{\bar{\alpha}}_d\right| \le c_\alpha$ and $\left|\dot{\bar{Q}}_d\right| \le c_Q$, respectively. Thus, based on (79), the following inequality holds

$$\begin{aligned}\chi_\alpha \dot{\chi}_\alpha + \chi_Q \dot{\chi}_Q \le & -\frac{\chi_\alpha^2}{\tau_\alpha} - \frac{\chi_Q^2}{\tau_Q} + \frac{a_\alpha^2}{2}\chi_\alpha^2 c_\alpha \\ & + \frac{1}{2a_\alpha^2} + \frac{a_Q^2}{2}\chi_Q^2 c_Q + \frac{1}{2a_Q^2}. \end{aligned} \tag{85}$$

Moreover,

$$\begin{aligned}\tilde{\varphi}\hat{\varphi} \ge & \frac{\tilde{\varphi}^2}{2} - \frac{\phi^2}{2}, S_\gamma \chi_\alpha + S_\alpha \chi_Q \\ \le & \frac{1}{2a_\gamma^2}S_\gamma^2 + \frac{a_\gamma^2 \chi_\alpha^2}{2} + \frac{1}{2a_\alpha^2}S_\alpha^2 + \frac{a_\alpha^2 \chi_Q^2}{2}, \end{aligned} \tag{86}$$

submitting (85) and (86) into (84) yields

$$\begin{aligned}\dot{Y} \le & -(k_V - 1)z_V^2 - k_h z_h^2 - k_\gamma S_\gamma^2 - k_\alpha S_\alpha^2 \\ & - \left(k_Q + \frac{1}{2a_Q^2}\right)S_Q^2 - (k_{\sigma_\phi} - 1)\sigma_\phi^2 \\ & - k_{\xi_\phi}\xi_\phi^2 - (k_{\sigma_{\delta_e}} - 1)\sigma_{\delta_e}^2 \\ & - k_{\xi_{\delta_e}}\xi_{\delta_e}^2 - \left(\frac{1}{\tau_\alpha} - \frac{a_\gamma^2}{2} - \frac{a_\alpha^2}{2}c_\alpha\right)\chi_\alpha^2 \\ & - \left(\frac{1}{\tau_Q} - \frac{a_\alpha^2}{2} - \frac{a_Q^2}{2}c_Q\right)\chi_Q^2 - \frac{b_V}{2}\left\|\tilde{w}_V^*\right\|^2 \\ & - \frac{1}{\lambda}\lambda\vartheta\tilde{\varphi}^2 + \frac{1}{2a_\gamma^2} + \frac{1}{a_\alpha^2} + \frac{1}{a_Q^2} + \frac{\delta_m^2}{2a_\gamma^2} \\ & + \frac{\delta_m^2}{2a_\alpha^2} + \frac{\delta_m^2}{2a_Q^2} + \frac{\delta_m}{4} + \frac{b_V}{2}\left\|w_V^*\right\|^2 + \frac{\vartheta\varphi^2}{2} \\ \le & -2\varepsilon Y + C, \end{aligned} \tag{87}$$

where

$$\begin{aligned} & k_V > 1,\ k_{\sigma_\phi} > 1,\ k_{\sigma_{\delta_e}} > 1,\ 0 < \tau_\alpha \\ & < \frac{2}{a_\gamma^2 + a_\alpha^2 c_\alpha}, 0 < \tau_Q < \frac{2}{a_\alpha^2 + a_Q^2 c_Q}, \\ & \varepsilon = \min\left\{\begin{array}{l} k_V - 1, k_h, k_\gamma, k_\alpha, k_Q + \frac{1}{2a_Q^2}, \\ k_{\sigma_\phi} - 1, k_{\xi_\phi}, k_{\sigma_{\delta_e}} - 1, k_{\xi_{\delta_e}}, \\ \frac{1}{\tau_\alpha} - \frac{a_\gamma^2}{2} - \frac{a_\alpha^2}{2}c_\alpha, \frac{1}{\tau_Q} - \frac{a_\alpha^2}{2} - \frac{a_Q^2}{2}c_Q, \\ \frac{b_V}{2\lambda_{\max}(\Gamma_V^{-1})}, \frac{\lambda\vartheta}{2} \end{array}\right\}, \\ & C = \frac{1}{2a_\gamma^2} + \frac{1}{a_\alpha^2} + \frac{1}{a_Q^2} + \frac{\delta_m^2}{2a_\gamma^2} + \frac{\delta_m^2}{2a_\alpha^2} + \frac{\delta_m^2}{2a_Q^2} + \frac{\delta_m}{4} \\ & + \frac{b_V}{2}\left\|w_V^*\right\|^2 + \frac{\vartheta\varphi^2}{2}. \end{aligned} \tag{88}$$

From (87), when $Y = \varsigma$, $\dot{Y} \le -2\varepsilon\varsigma + C$, if $\varepsilon > \frac{C}{2\varsigma}$, then $\dot{Y} \le 0$ on $Y = \varsigma$, so $Y \le \varsigma$ is an invariant set, i.e., if $Y(0) \le \varsigma$, then $Y(t) \le \varsigma$ for all $t \ge 0$. Therefore, the inequality (87) holds for all $Y(t) \le \varsigma$ and $t \ge 0$.

Standard arguments can now be applied to solve the differential inequality (87) as follows

$$0 \le Y(t) \le \frac{C}{2\varepsilon} + (Y(0) - \frac{C}{2\varepsilon})\exp(-2\varepsilon t), \forall t \ge 0, \tag{89}$$

it is obvious that $Y(t)$ is bounded by $\frac{C}{2\varepsilon}$, i.e., for $t \ge 0, 0 \le Y(t) \le \frac{C}{2\varepsilon}$. It can be concluded that $z_V, z_h, S_\gamma, S_\alpha, S_Q, \sigma_\phi, \xi_\phi, \sigma_{\delta_e}, \xi_{\delta_e}, \chi_\alpha, \chi_Q, \tilde{w}_V^*$, and $\tilde{\varphi}$ are semi-globally uniformly ultimate boundedness.

In what follows, it can be shown that the respective velocity and altitude tracking errors can converge to arbitrarily small neighborhoods around zero by suitably choosing the controller parameters.

From inequality (89), the velocity and altitude tracking errors yield

$$\begin{aligned} |z_V| \le & \sqrt{\frac{C}{\varepsilon} + \left(2Y(0) - \frac{C}{\varepsilon}\right)\exp(-2\varepsilon t)}, \\ |z_h| \le & \sqrt{\frac{C}{\varepsilon} + \left(2Y(0) - \frac{C}{\varepsilon}\right)\exp(-2\varepsilon t)}, \ \forall t \ge 0, \end{aligned} \tag{90}$$

thus

$$\lim_{t\to\infty}|z_V| \le \sqrt{C/\varepsilon}\ ,\ \lim_{t\to\infty}|z_h| \le \sqrt{C/\varepsilon}, \tag{91}$$

then the convergence domains of z_V and z_h can be expressed as the following compact sets

$$\begin{aligned} R_V &= \left\{ z_V \,\middle|\, |z_V| \le \sqrt{C/\varepsilon} \right\}, \\ R_h &= \left\{ z_h \,\middle|\, |z_h| \le \sqrt{C/\varepsilon} \right\}. \end{aligned} \tag{92}$$

From (92), the altitude and altitude tracking errors can converge to arbitrarily small neighborhoods around zero by increasing ε sufficiently large, which can be achieved by properly choosing the design parameters in (88), i.e., a_γ, a_α, a_Q, b_V, and ϑ are fixed such that C in (88) is independent of ε. Then, we can choose k_V, k_h, k_γ, $k_\alpha, k_Q, \lambda, k_{\sigma_\phi}, k_{\xi_\phi}, k_{\sigma_{\delta_e}}$, and $k_{\xi_{\delta_e}}$ large enough and $\tau_\alpha, c_\alpha, \tau_Q, c_Q$, and $\lambda_{\max}(\Gamma_V^{-1})$ small enough to obtain large ε. In this way, the value of C/ε can be arbitrarily small. Therefore, it can be concluded that by appropriately choosing the parameters, the velocity and altitude tracking errors can converge to arbitrarily small neighborhoods around zero.

Remark 7 In the above sections, the controller design and stability analysis are based on the consideration of input constraint. If it is not taken into account, the control inputs are designed as

$$\phi_c = -k_V z_V + \dot{V}_d - \frac{z_V \mu_\phi(z_V)}{\xi_\phi^2 + z_V^2} - \hat{w}_V^{*T}\xi_V, \tag{93}$$

$$\begin{aligned} \delta_{ec} = &-\left(\frac{1}{2a_Q^2} + \frac{a_Q^2}{2}\right) S_Q - k_Q S_Q + \dot{Q}_d \\ &- \frac{S_Q \mu_{\delta_e}(S_Q)}{\xi_{\delta_e}^2 + S_Q^2} - \frac{a_Q^2}{2} S_Q \hat{\varphi} \xi_Q^T \xi_Q - S_\alpha. \end{aligned} \tag{94}$$

In the following section, we will compare the simulation results of different scenarios where input constraints are considered and not considered.

Table 2 Initial flight condition of the FAHV

State	Value	State	Value
h(ft)	85000	$\dot{\eta}_2$	0
V(ft/s)	7846	$\dot{\eta}_3$	0
γ(rad)	0	η_1	0.56196
α(rad)	0.0175	η_2	−0.057072
Q(rad/s)	0	η_3	−0.029406
$\dot{\eta}_1$	0		

Table 3 Control input constraints

Control input	Lower bound	Upper bound
ϕ	0.1	1.2
δ_e(rad)	−0.2618	0.2618

5 Simulations

In this section, the performance of the developed control strategy applied to the CFM model (1)–(6) is verified by means of simulations. The vehicle model parameters are referred from [50]. The fuel level is assumed at 50 %. The initial flight condition of the vehicle is given in Table 2. The limits are deliberately tightened to explore the capability of the designed controller in adhering to the limits. The constraints used are shown in Table 3. Reference commands are smoothened via a second-order transfer function with a natural frequency $\omega_f = 0.03rad/s$ and a damping ratio $\xi_f = 0.95$. The parameters adopted for control inputs, adaptive laws, and additional systems are given in Table 4. The following four scenario simulations are performed to test the performance of the designed controller in handling input constraints and aerodynamic uncertainty. To demonstrate the robustness of the proposed control scheme, two types of aerodynamic uncertainty are considered. CaseI: *30 % uncertainty* of the aerodynamic parameters is taken into account. CaseII: *20 % uncertainty*of the aerodynamic parameters is considered.

Table 4 Parameters of the controller

Parameter	Value	Parameter	Value	Parameter	Value	Parameter	Value
k_V	20	b_V	0.01	k_Q	12	a_γ, a_α, a_Q	1
k_{σ_ϕ}	1.2	k_h	2	$\psi_V, \psi_Q, \psi_\phi, \psi_{\delta_e}$	0.0001	λ	20
k_{ξ_ϕ}	0.0001	k_γ	5	$k_{\xi_{\delta_e}}$	2	$k_{\sigma_{\delta_e}}$	2
Γ_V	10	k_α	4	τ_α, τ_Q	0.05	ϑ	0.0002

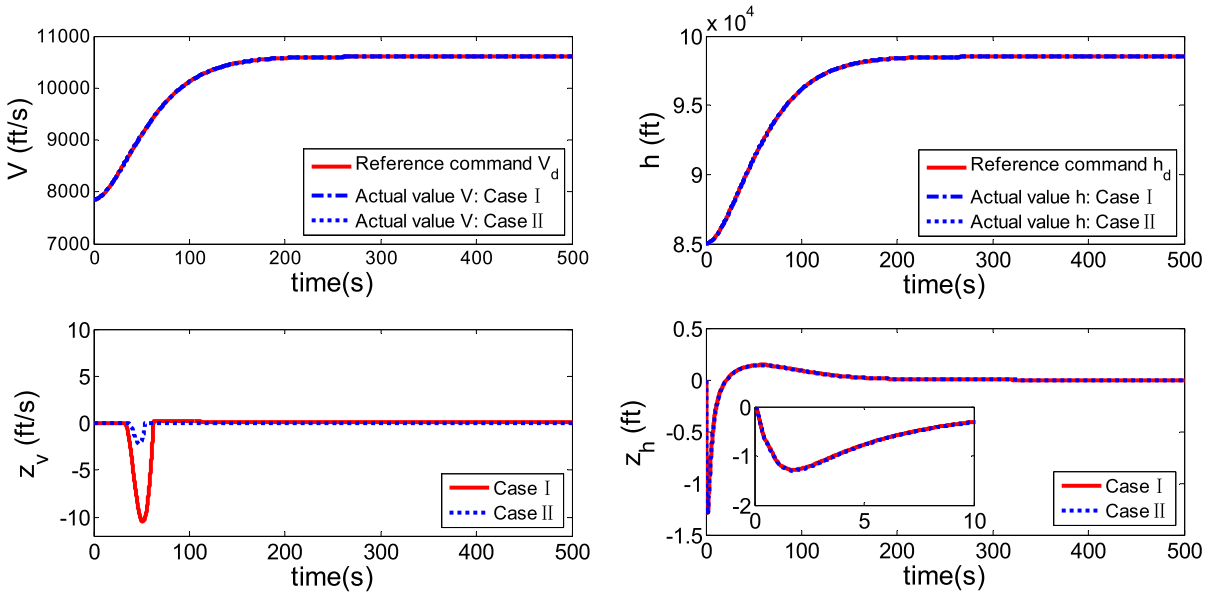

Fig. 2 Time responses of velocity, altitude, velocity tracking error, and altitude tracking error in Scenario 1. **a** Velocity V, **b** altitude h, **c** velocity tracking error z_V, **d** altitude tracking error z_h

Scenario 1 Input constraints and aerodynamic uncertainty are considered at the level of control design. In this scenario, it is a climbing maneuver with longitudinal acceleration, in which the altitude and velocity reference commands are chosen independently. The altitude reference command h_d is generated to make the vehicle climb from 85,000 to 98,500 ft, and the velocity reference command V_d is generated to make the vehicle accelerate from 7846 to 10,600 ft/s. The time responses of applying control inputs (31) and (68) to the CFM (1)–(6) to track the altitude and velocity reference commands are shown in Figs. 2, 3, and 4. From the simulation result, we can obtain that the designed controller can achieve a good tracking performance.

It is apparent from Fig. 2 that altitude and velocity stably follow their respective reference commands. The velocity accelerates to 10,600 ft/s and the altitude climbs to 98,500 ft in about 200 s. In case I, the maximum absolute values of the velocity and altitude tracking errors are less than 11 ft/s and 1.5 ft, respectively. In case II, the maximum absolute values of the velocity altitude tracking errors are less than 2.5 ft/s and 1.5 ft, respectively. As can be observed from Fig. 3, the altitude tracks the reference command via the stable tracking of FPA reference command. The maximum absolute values of FPA tracking errors are less than 0.0004 rad in both two uncertain cases. The maximum absolute values of velocity, altitude, and FPA tracking errors are much smaller than the magnitude of their reference commands. The control inputs that realize the stable tracking of the reference commands are demonstrated in Fig. 4. The saturation occurs in the fuel equivalence ratio, while elevator deflection remains within constraint in both the uncertain cases. During the saturation phase, the tracking performance degrades as given in Fig. 2. As shown in Fig. 4, the term $k_V \sigma_\phi$ makes the fuel equivalence ratio return to the linear work space after about 53 and 63 s in case I and case II, respectively. The designed controller recovers its tracking performance after it comes out of saturation phase as can be seen from Fig. 2. Moreover, as shown in Fig. 4, three flexible states converge to their stable values despite excitations.

Based on the simulation results of Scenario 1, the following conclusions can be obtained. (a) Under the same controller parameters and simulation condition, different types of aerodynamic uncertainty have obviously different effects on the tracking performance of velocity. The maximum absolute value of the velocity tracking error increases as the uncertainty increases. While in the two uncertain cases, the tracking performance of altitude has no obvious change. (b) The

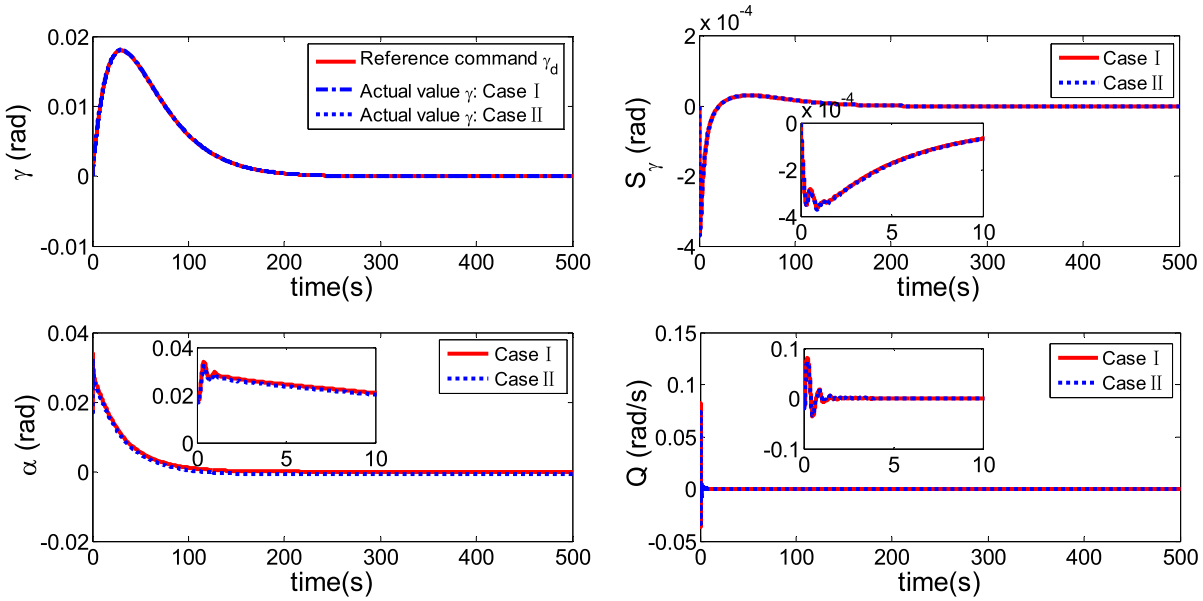

Fig. 3 Time responses of FPA, FPA tracking error, AOA, and pitch rate in Scenario 1. **a** FPA γ, **b** FPA tracking error S_γ, **c** AOA α, **d** pitch rate Q

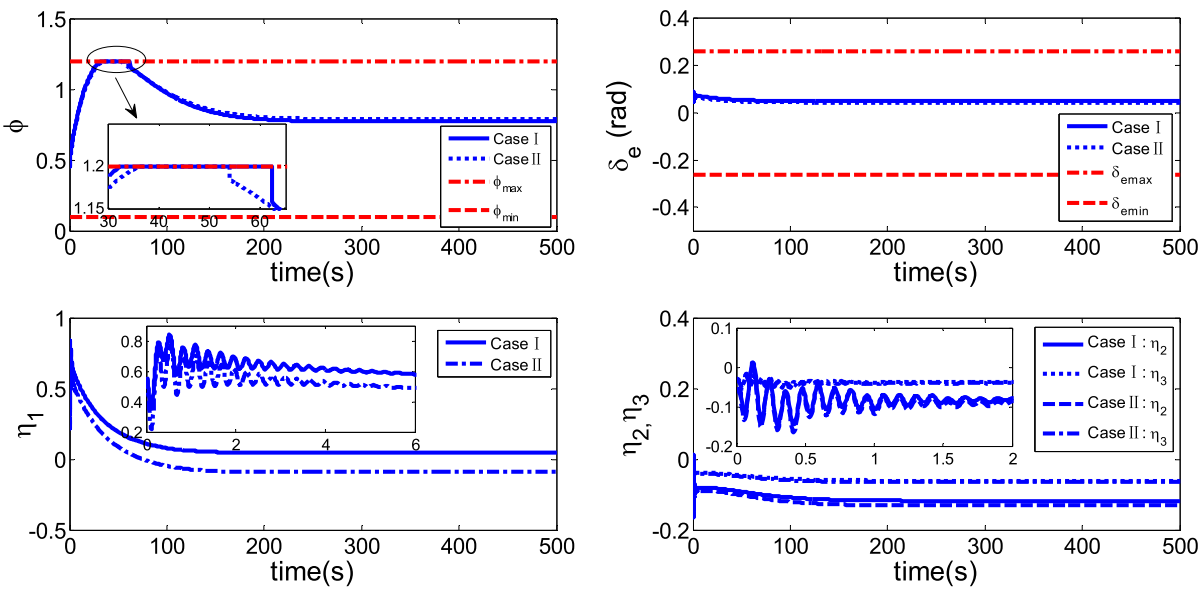

Fig. 4 Time responses of control inputs: fuel equivalence ratio, elevator deflection, and flexible states in Scenario 1. **a** Fuel equivalence ratio ϕ, **b** elevator deflection δ_e, **c** flexible state η_1, **d** flexible state s η_2, η_3

time of saturation phase increases as the uncertainty increases.

To show the efficiency of the proposed control method in tackling input constraints, the controller without considering input constraint is also employed in the simulation studies for the purpose of comparison.

Scenario 2 In this scenario, input constraint is not taken into consideration at the level of control design but manually included at the level of simulation.

The above-mentioned two cases of uncertainty are considered. Reference commands are chosen the same

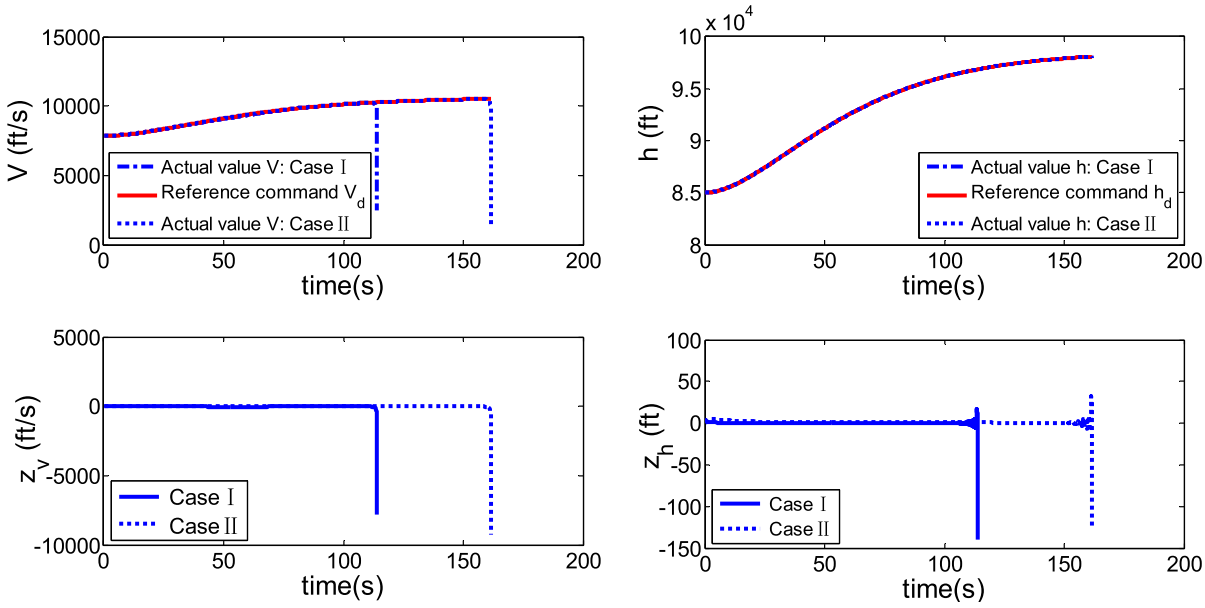

Fig. 5 Time responses of velocity, altitude, velocity tracking error, and altitude tracking error in Scenario 2. **a** Velocity V, **b** altitude h, **c** velocity tracking error z_V, **d** altitude tracking error z_h

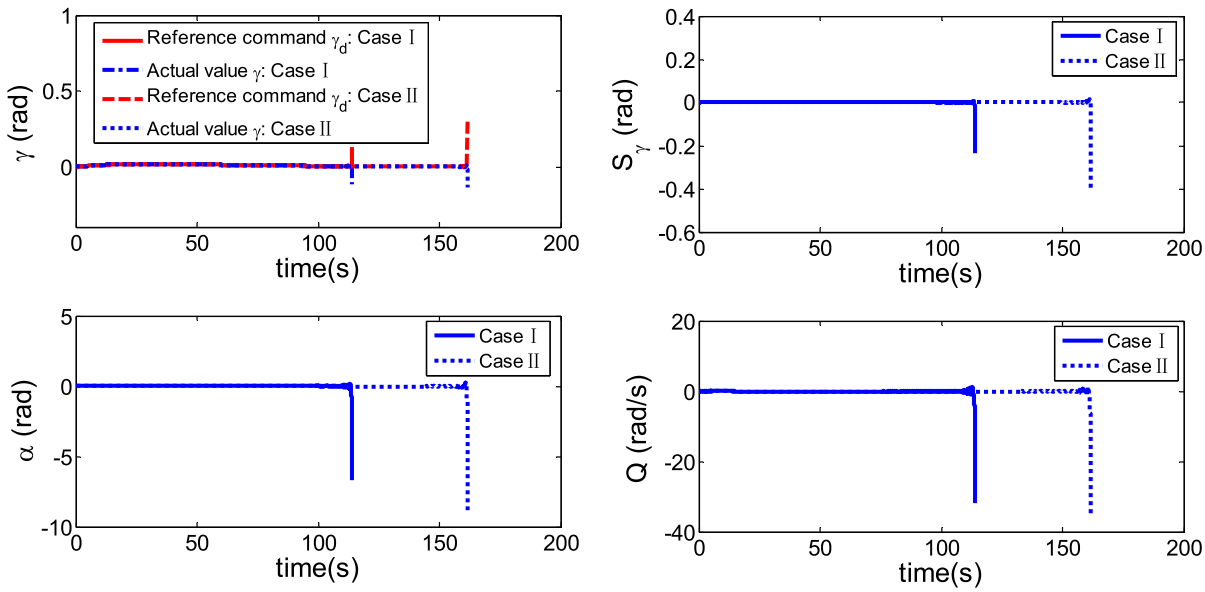

Fig. 6 Time responses of FPA, FPA tracking error, AOA, and pitch rate in Scenario 2. **a** FPA γ, **b** FPA tracking error S_γ, **c** AOA α, **d** pitch rate Q

as that of Scenario 1. The controller is designed as that given in Remark 7. The time responses of applying control inputs (93) and (94) to the CFM (1)–(6) are presented in Figs. 5, 6, and 7. It is clear that the system becomes unstable as the control inputs hit their saturation in both the uncertain cases. Moreover, it can be observed that the speed of the control inputs which violate their limits increases as the uncertainty increases.

In Scenario 1 and 2, an aggressive maneuver is considered. Dynamic pressure is changing. In order to

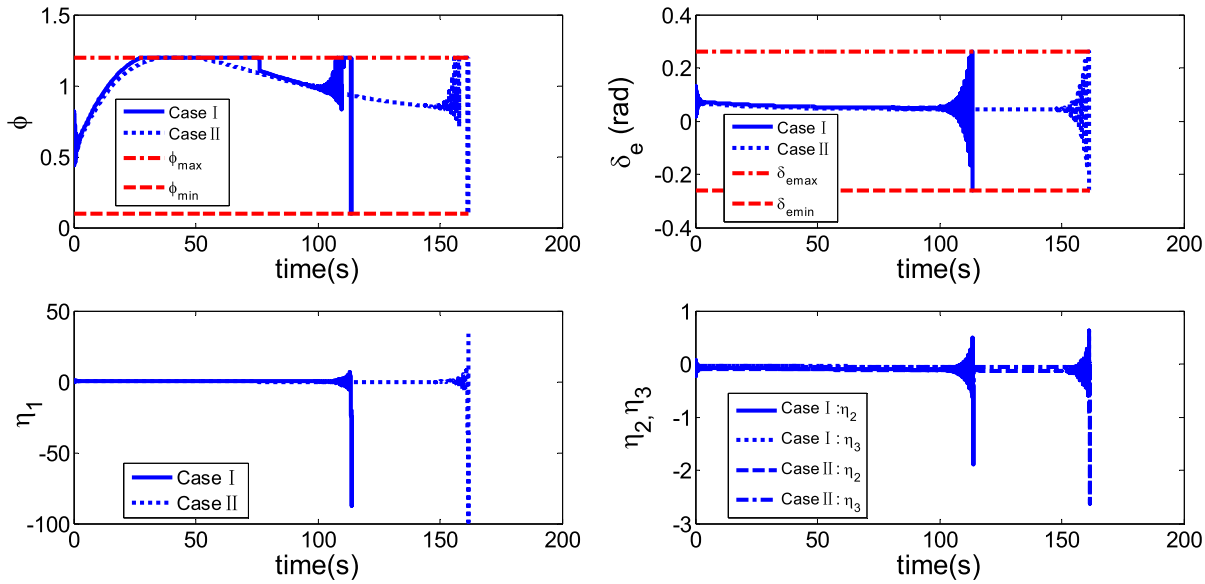

Fig. 7 Time responses of control inputs: fuel equivalence ratio, elevator deflection, and flexible states in Scenario 2. **a** Fuel equivalence ratio ϕ, **b** elevator deflection δ_e, **c** flexible state η_1, **d** flexible states η_2, η_3

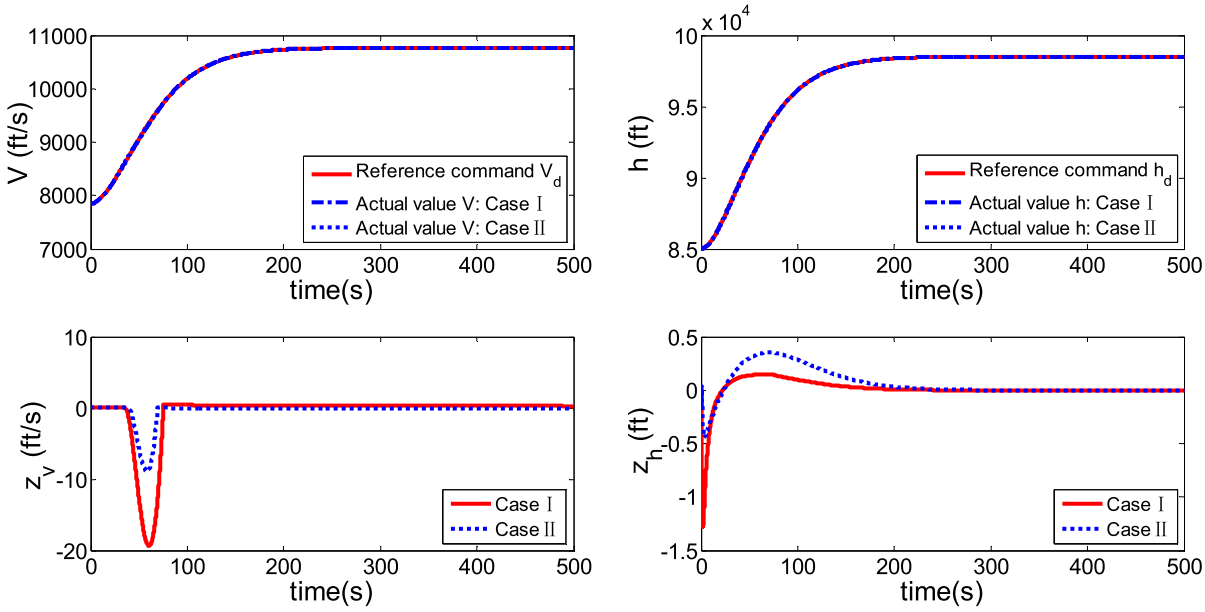

Fig. 8 Time responses of velocity, altitude, velocity tracking error, and altitude tracking error in Scenario 3. **a** Velocity V, **b** altitude h, **c** velocity tracking error z_V, **d** altitude tracking error z_h

better present the effectiveness and feasibility of the designed control strategy, we carry the scenarios that dynamic pressure is constant.

Scenario 3 In this scenario, input constraints and aerodynamic uncertainty are considered simultaneously. Two uncertain cases (cases I and II) are also taken into account. However, the flight mission is different from Scenario 1. It is a climbing maneuver at constant dynamic pressure. The altitude reference command h_d is generated to make the vehicle climb from 85,000 to 98,500 ft, whereas the velocity reference

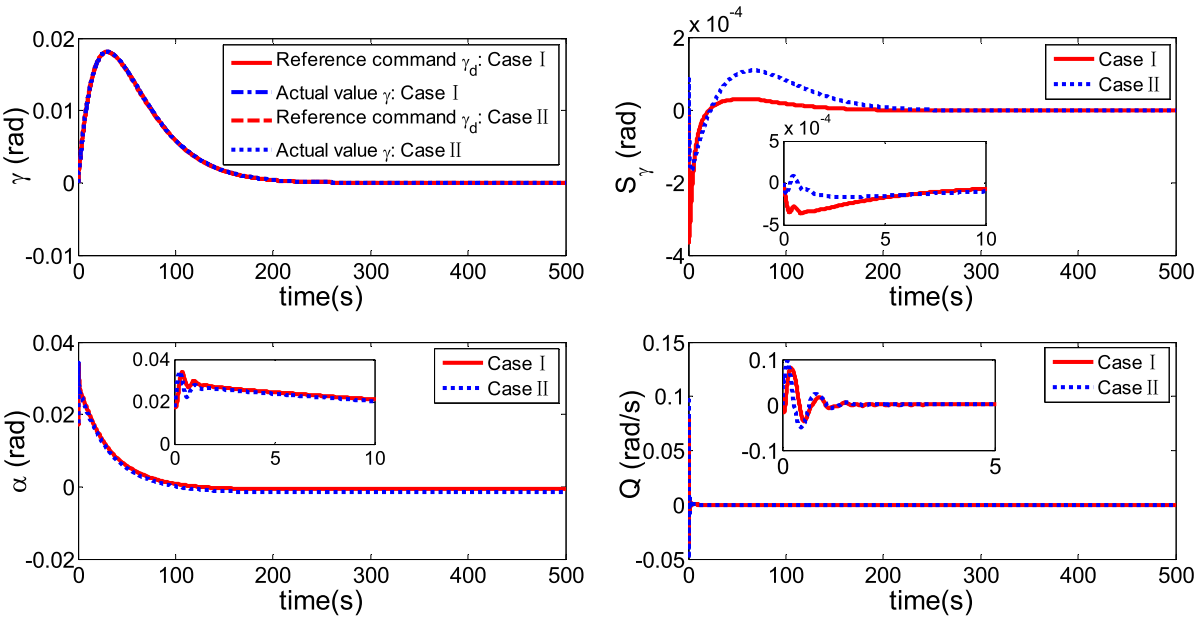

Fig. 9 Time responses of FPA, FPA tracking error, AOA, and pitch rate in Scenario 3. **a** FPA γ, **b** FPA tracking error S_γ, **c** AOA α, **d** pitch rate Q

command V_d is computed according to the relation $V_d = (2\overline{q}\exp((h_d - h_0)/h_s)/\rho_0)^{(0.5)}$ to maintain the constant dynamic pressure at 2075.44 psf during the entire maneuver. The time responses of Scenario 3 are shown in Figs. 8, 9, and 10.

From the simulation results, it can be observed that the designed control strategy achieves the good tracking performance. As shown in Fig. 8, altitude and velocity stably follow their reference commands, respectively. The vehicle climbs 13,500 ft in about 295 s, while the velocity accelerates about 2,916 ft/s. The tracking errors of velocity and altitude all converge to the small neighborhoods around zero. The altitude converges to its reference command through the stable tracking of FPA reference command. The maximum absolute values of the velocity, altitude, and FPA tracking errors are also much smaller than those of reference commands. It is obvious from Fig. 10 that the input saturation only occurs in fuel equivalence ratio. Moreover, the flexible states converge to stable values despite excitations.

Correspondingly, for comparison, simulation of the following scenario is carried out.

Scenario 4 In this scenario, we do the simulation that applies the RBFNN-based robust adaptive DSC controller (93) and (94) to the CFM (1)–(6). The input constraints are included manually at the level of simulation instead of at the level of control design.

In this scenario, aerodynamic uncertainty is taken into account. The time responses are depicted in Figs. 11, 12, and 13 which exhibit the similar control performance shown in Scenario 2. It is clear that the system becomes unstable as the inputs hit their limits.

We can obtain the following conclusions based on the above simulation results of four scenarios. On the basis of the simulation results of Scenario 2 and 4, all the variables under the designed controller tend to be unstable, which implies that input constraint should be considered during the controller design procedure instead of manually implementing at the level of simulation. It is concluded from the simulation results of Scenario 1 and 3 that the designed control strategy can handle input constraint effectively. The input saturation only occurs in the fuel equivalence ratio. Elevator deflection always keeps in their limits. Though the maximum absolute values of altitude, velocity, and FPA tracking errors occur during the saturation phase of the fuel equivalence ratio, they are much smaller than those of reference commands.

Although the vehicle climbs 13,500 ft in both two scenarios, we can obtain that the velocity acceler-

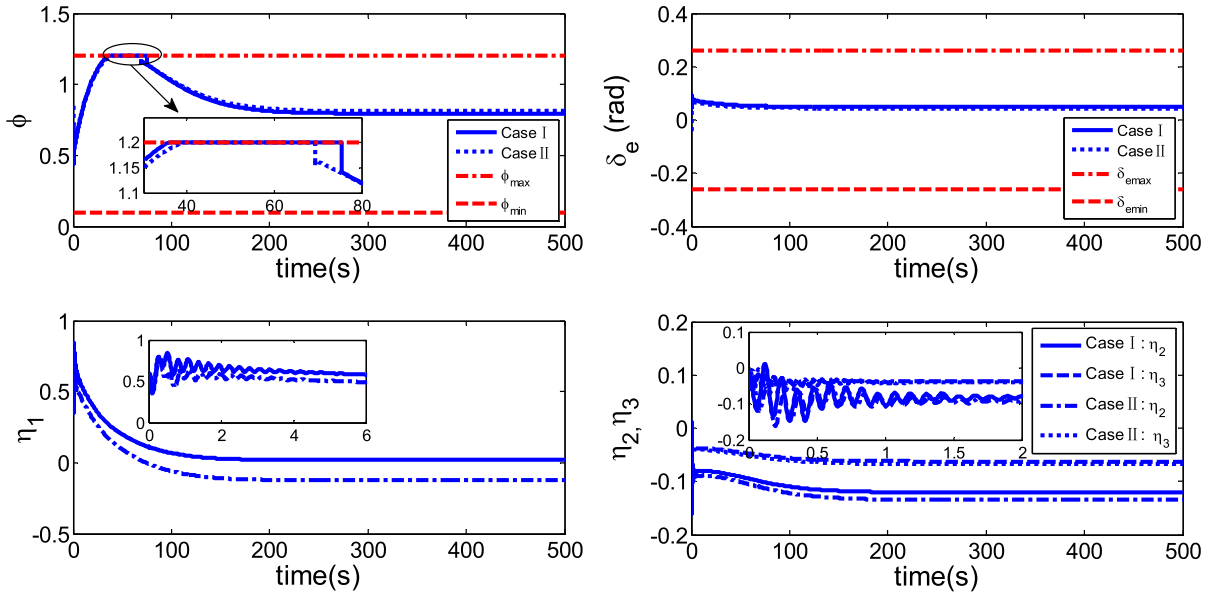

Fig. 10 Time responses of control inputs: fuel equivalence ratio, elevator deflection, and flexible states in Scenario 3. **a** Fuel equivalence ratio ϕ, **b** elevator deflection δ_e, **c** flexible state η_1, **d** flexible states η_2, η_3

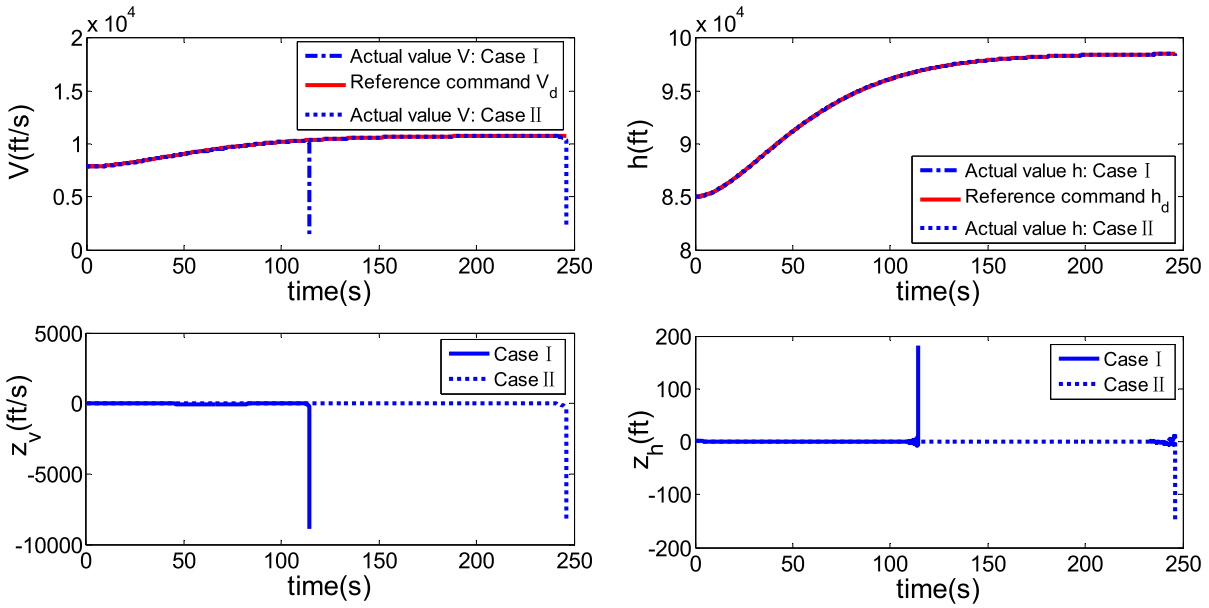

Fig. 11 Time responses of velocity, altitude, velocity tracking error, and altitude tracking error in Scenario 4. **a** Velocity V, **b** altitude h, **c** velocity tracking error z_V, **d** altitude tracking error z_h

ates to 10 762 ft/s in Scenario 3 from the relation $V_d = (2\overline{q}exp((h_d - h_0)/h_s)/\rho_0)^{(0.5)}$. It is more than that of Scenario 1, where the velocity accelerates to 10,600 ft/s. From the simulation results of Scenario 1 and 3, we can conclude the following three aspects:

(a) For the two uncertain cases, the maximum absolute values of the velocity tracking error in Scenario 1 are all less than those of Scenario 3. However, the maximum absolute value of the altitude tracking error in Scenario 1 is nearly the same as that of

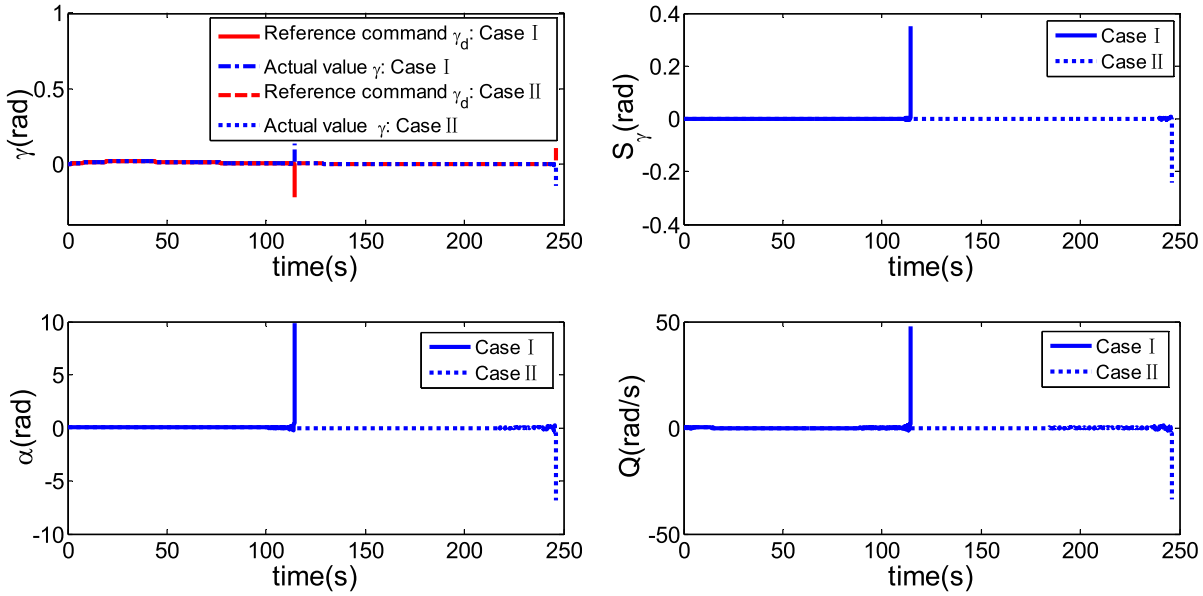

Fig. 12 Time responses of FPA, FPA tracking error, AOA, and pitch rate in Scenario 4. **a** FPA γ, **b** FPA tracking error S_γ, **c** AOA α, **d** pitch rate Q

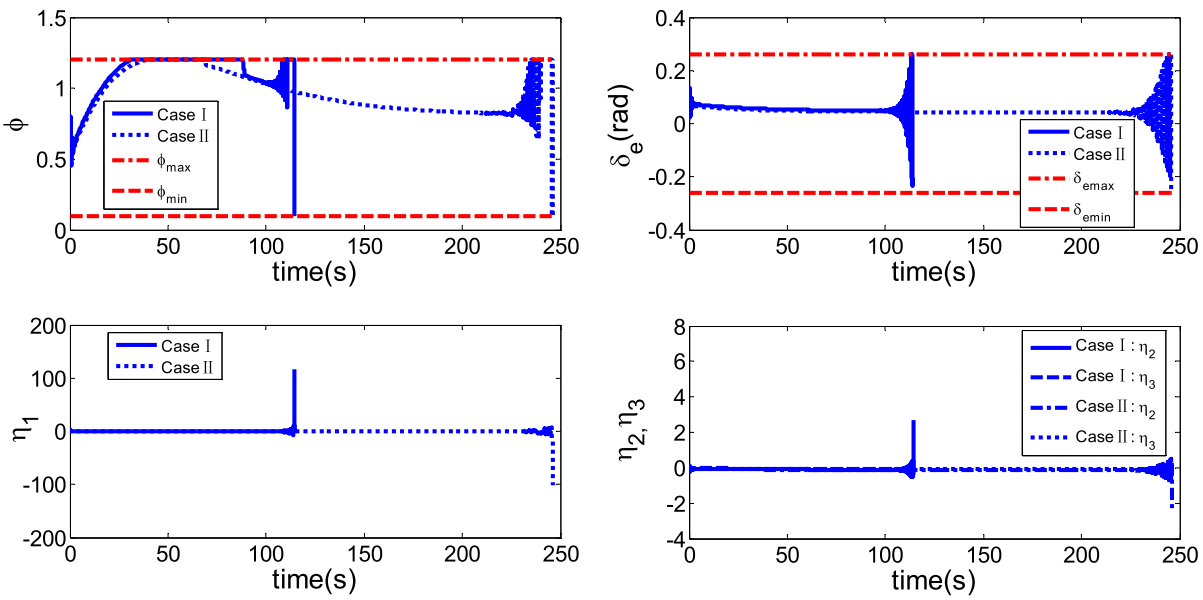

Fig. 13 Time responses of control inputs: fuel equivalence ratio, elevator deflection, and flexible states in Scenario 4. **a** Fuel equivalence ratio ϕ, **b** elevator deflection δ_e, **c** flexible state η_1, **d** flexible states η_2, η_3

Scenario 3. The time of saturation phases in Scenario 1 is shorter than that of Scenario 3.

(b) In both two scenarios, the maximum absolute value of the velocity tracking error and the time of saturation phase increases as the uncertainty increases.

Remark 8 In Sect. 4, the value $\sqrt{C/\varepsilon}$ in (92) is only a theoretical bound and cannot be computed in practical applications because of some unknown parameters such as δ_m, w_V^*, and ϑ. Since some inequalities are employed in the stability analysis, this bound may

be conservative. However, from the simulation results in the subsequent section, the bounds of altitude and velocity tracking errors are very small. Besides, from the above stability analysis, if the gains are chosen appropriately, it is possible to make C/ε as small as desired and thus achieving regulation to a small neighborhood around zero. The bound C/ε can be reduced by increasing the gains k_V, k_h, k_γ, k_α, k_Q, λ, k_{σ_ϕ}, k_{ξ_ϕ}, $k_{\sigma_{\delta_e}}$, and $k_{\xi_{\delta_e}}$ or decreasing gains τ_α, c_α, τ_Q, c_Q, and $\lambda_{\max}(\Gamma_V^{-1})$. However, from a practical review, it should be pointed out that increasing the gains can decrease the bound of tracking error, but it would result in a variation of a high-gain control scheme. It not only makes transient performance deteriorate, but also excites any unmodeled dynamics of the system. So, the designer should suitably choose the gains to make sure that the steady-state tracking error can satisfy the practical requirement, while keeping gains as small as possible to obtain the ideal transient performance.

The simulation results of the above four scenarios indicate that it is necessary to consider input constraint during the controller design procedure. Under the designed robust adaptive DSC control scheme, though there are input constraint and aerodynamic uncertainty, the desired tracking performance can be ensured and satisfactory system responses can be achieved. We can conclude that the proposed controller could simultaneously deal with uncertainty and input constraints (21)–(22) effectively.

6 Conclusions

A robust adaptive dynamic surface controller based on RBFNN is developed for a nonlinear longitudinal model of FAHV, where input constraints and aerodynamic uncertainty are taken into consideration. At first, COM is derived from CFM and its equations of motion are decomposed into velocity subsystem and altitude subsystem to reduce the controller design complexity. The flexible dynamics are taken as the perturbations of the COM, and their effects are evaluated through simulation. Then the RBFNN-based robust adaptive control scheme is designed for the velocity subsystem; the RBFNN-based robust adaptive DSC control scheme is developed for the altitude subsystem. At the level of control design, MLP technique is employed to estimate the maximum norm of the ideal weight vectors of RBFNN rather than their elements. It leads to the large reduction of the computational burden. The problem posed by input constraints is overcome by additional systems. Their states are utilized for the controller design and stability analysis. By suitably choosing controller parameters, the designed control strategy assures that the velocity and altitude tracking errors can be very small even in the presence of aerodynamic uncertainty and input constraint. The compared simulations illustrate that the designed controller achieves robust and stable tracking properties. In the paper, we assume that all rigid body states of FAHV are measured, but it may be hard to measure some states such as AOA and FPA. Our further work will focus on the flight control problem of FAHV with input constraints and part states unmeasured.

Acknowledgments The authors would like to greatly appreciate the editor and all anonymous reviewers for their comments, which help to improve the quality of this paper. This work was supported in part by the National Natural Science Foundation of China (61203012 and 61273092), Key Grant Project of Chinese Ministry of Education (311012), Tianjin Basic Research Key Foundation (11JCZDJC25100), and Aeronautical Science Foundation of China (20125848004) Supported by Science and Technology on Aircraft Control Laboratory. It was also supported by the Tianjin Key Laboratory of Process Measurement and Control (TKLPMC-201315) Independent Innovation Fund of Tianjin University (2013XQ-0022).

References

1. Bolender, M.A., Doman, D.B.: A nonlinear longitudinal dynamical model of an air-breathing hypersonic vehicle. J. Spacecr. Rocket **44**(2), 374–387 (2007)
2. Sun, H.B., Li, S.H., Sun, C.Y.: Finite time integral sliding mode control of hypersonic vehicles. Nonlinear Dyn. **73**(1–2), 229–244 (2013)
3. Groves, K.P., Serrani, A., Yurkovich, S., Bolender, M.A., Doman, D.B.: Anti-windup control for an air-breathing hypersonic vehicle model. In: AIAA Guidance, Navigation, and Control Conference and Exhibit, Keystone, Colorado, 21–24 Aug, AIAA 2006–6557 (2006)
4. Fiorentini, L., Serrani, A., Bolender, M.A., Doman, D.B.: Robust nonlinear sequential loop closure control design for an air-breathing hypersonic vehicle model. In: American Control Conference, American Automatic Control Council, Dayton, 3458–3463 (2008)
5. Xu, H.J., Maj, D.M., Petros, A.I.: Adaptive sliding mode control design for a hypersonic flight vehicle. J. Guid. Control Dyn. **27**(5), 829–838 (2004)
6. Cai, G.B., Duan, G.R., Hu, C.H.: Neural network-based adaptive dynamic surface control for an airbreathing hypersonic vehicle. In: Proceedings of the 3rd International Symposium on Systems and Control in Aeronautics and Astro-

nautics (ISSCAA), 8–10 June, Harbin, Hei Longjiang, 598–603 (2010)
7. Morelli, E.A.: Flight test experiment design for characterizing stability and control of hypersonic vehicles. In: U.S. Air Force T&E Days, AIAA-2008-1682, Los Angeles, Feb (2008)
8. Li, S.H., Sun, H.B., Sun, C.Y.: Composite controller design for an airbreathing hypersonic vehicle. Proc. Inst. Mech. Eng. Part I **226**(5), 651–664 (2012)
9. Sun, H.B., Li, S.H., Sun, C.Y.: Robust adaptive integral-sliding-mode fault-tolerant control for air-breathing hypersonic vehicles. Proc. Inst. Mech. Eng. Part I **226**(10), 1344–1355 (2012)
10. Rodriguez, A.A., Dickeson, J.J., Sridharan, S., et al.: Control-relevant modeling, analysis, and design for scramjet-powered hypersonic vehicles. In: AIAA/DLR/DGLR International Space Planes and Hypersonic Systems and Technologies Conference, AIAA-2009-7287 (2009)
11. Yang, J., Li, S.H., Sun, C.Y., Guo, L.: Nonlinear-disturbance-observer-based robust flight control for air-breathing hypersonic vehicles. IEEE Trans. Aerosp. Electron. Syst. **49**(2), 1263–1275 (2013)
12. Levin, J.M., Ioannou, P., Mirmirani, M.: Adaptive mode suppression scheme for an aeroelastic airbreathing hypersonic cruise vehicle. In: AIAA Guidance, Navigation, and Control Conference. and Exhibit, Reston (2008)
13. Fidan, B., Mirmirani, M., Ioannou, P.: Flight dynamics and control of air-breathing hypersonic vehicles: review and new directions. In: AIAA International Space Planes and Hypersonic Systems and Technologies, Reston (2003)
14. Bolender, M.A., Doman, D.B.: A non-linear model for the longitudinal dynamics of a hypersonic air-breathing vehicle. In: AIAA Guidance, Navigation and Control Conference and Exhibit, San Francisco, 15–18 Aug, AIAA-2006-6557 (2005)
15. Parker, J.T., Serrani, A., Yurkovich, S., et al.: Control-oriented modeling of an air-breathing hypersonic vehicle. J. Guid. Contrtol Dyn. **30**(3), 856–868 (2007)
16. Adami, T.M., Sabala, R., Zhu, J.J.: Time-varying notch filters for control of flexible structures and vehicles. In: Proceedings of the 22nd Digital Avionics Systems Conference, Indianapolis, 12–16 Oct, 7.C.2– 7.1-6 vol. 2 (2003)
17. Adami, T.M., Zhu, J.J.: Control of a flexible, hypersonic scramjet vehicle using a differential algebraic approach. In: AIAA Gguidance, Navigation, and Control Conference and Exhibit, Honolulu, 18–21 Aug, AIAA-2008-746 (2008)
18. Levin, J.M., Ioannou, P., Mirmirani, M.: Adaptive mode suppression scheme for an aeroelastic airbreathing hypersonic cruise vehicle. In: AIAA Guidance, Navigation, and Control Conference and Exhibit, Honolulu, 18–21 Aug, AIAA-2008-7464 (2008)
19. Rehman, O., Fidan, B., Petersen, I.R.: Uncertainty modeling and robust minimax LQR control of hypersonic flight vehicles. In: AIAA Guidance, Navigation, and Control Conference, 2–5 Aug, AIAA-2010-8285 (2010)
20. Rehman, O., Petersen, I.R., Fidan, B.: Robust nonlinear control design of a hypersonic flight vehicle using minimax linear quadratic Gaussian control. In: Proceedings of the 49th IEEE Conference on Decision and Control, IEEE, New York, 6219–6224 (2010)
21. Wilcox, Z.D., MacKunis, W., Bhat, S., Lind, R., Dixon, W.E.: Lyapunov-based exponential tracking control of a hypersonic aircraft with aerothermoelastic effects. J. Guid. Control Dyn. **33**(4), 1213–1221 (2010)
22. Hu, X.X., Gao, H.J., Karimi, H.R., Wu, L.G., Hu, C.H.: Fuzzy reliable tracking control for flexible air-breathing hypersonic vehicles. Int. J. Fuzzy Syst. **13**(4), 323–334 (2011)
23. Hu, X.X., Wu, L.G., Hu, C.H., et al.: Adaptive sliding mode tracking control for a flexible air-breathing hypersonic vehicle. J. Frank. Inst. **349**(2), 559–577 (2012)
24. Sun, H.F., Yang, Z.L., Zeng, J.P.: New tracking-control strategy for airbreathing hypersonic vehicles. J Guid. Control Dyn. **36**(3), 846–859 (2013)
25. Lei, Y., Cao, C. Y., Cliff, E., et al.: Design of an L_1 adaptive controller for air-breathing hypersonic vehicle model in the presence of unmodeled dynamics. In: AIAA Guidance, Navigation, and Control Conference and Exhibit, Hilton Head, South Carolina, 20–23 Aug, AIAA-2007-6527 (2007)
26. Kharisov, E., Gregory, I.M., Cao, C.Y., et al.: L_1 adaptive control for flexible space launch vehicle and proposed plan for flight validation. In: AIAA Guidance, Navigation, and Control Conference and Exhibit, Honolulu, 18–21 Aug, AIAA-2008-7128 (2008)
27. Lei, Y., Cao, C.Y., Cliff, E., et al.: L_1 adaptive controller for air-breathing hypersonic vehicle with flexible body dynamics. In: American Control Conference, Virginia Tech, Blacksburg, 10–12 June (2009)
28. Fiorentini, L., Serrani, A., Bolende, M.A., Doman, D.B.: Nonlinear robust/adaptive controller design for an airbreathing hypersonic vehicle model. In: AIAA Guidance, Navigation, and Control Conference and Exhibit, Hilton Head, 20–23 Aug, AIAA-2007-632 (2007)
29. Fiorentini, L., Serrani, A., Bolender, M.A., Doman, D.B.: Nonlinear control of a hypersonic vehicle with structural flexibility. In: Proceedings of the 47th IEEE Conference on Decision and Control, Cancun, 9–11 Dec, 578–583 (2008)
30. Fiorentini, L., Serrani, A., Bolender, M.A., Doman, D.B.: Nonlinear robust adaptive control of flexible air-breathing hypersonic vehicles. J. Guid. Control Dyn. **32**(2), 401–415 (2009)
31. Serrani, A., Zinnecker, A.M., Fiorentini, L., Bolender, M.A., Doman, D.B.: Integrated adaptive guidance and control of constrained nonlinear air-breathing hypersonic vehicle models. In: American Control Conference, Hyatt Regency, Riverfront, St. Louis, June 10–12, 3172–3177 (2009)
32. Jonhson, E., Calise, A.: Limited authority adaptive flight control for reusable launch vehicles. J. Guid. Control Dyn. **26**(6), 906–913 (2003)
33. Lavretsky, E., Hovakimyan, N.: Stable adaptation in the presence of actuator constraints with flight control applications. J. Guid. Control Dyn. **30**(2), 337–345 (2007)
34. Zinnecker, A., Serrani, A., Bolender, M.A., Doman, D.B.: Combined reference governor and anti-windup design for constrained hypersonic vehicles models. In: AIAA Guidance, Navigation, and Control Conference, Chicago, 10–12 Aug, AIAA-2009-6283 (2009)
35. Recasens, J.J., Chu, Q.P., Mulder, J.A.: Robust MPC of a feedback linearized, system for a lifting-body reentry vehicle. In: AIAA Guidance, Navigation and Control Conference

and Exhibit, San Francisco, 15–18 Aug, AIAA-2005-6147 (2005)
36. Van Soest, W.R., Chu, Q.P., Mulder, J.A.: Combined feedback linearization and constrained model predictive control for entry flight. J. Guid. Control Dyn. **29**(2), 427–434 (2006)
37. Vaddi, S.S., Sengupta, P.: Controller design for hypersonic vehicles accommodating nonlinear state and control constraints. In: AIAA Guidance, Navigation and Control Conference, Chicago, 10–12 Aug, AIAA-2009-6286 (2009)
38. Gao, Y.: Linear feedback guidance for low-thrust many-revolution earth-orbit. J. Spacecr. Rockets **46**(6), 1320–1325 (2009)
39. Gao, G., Wang, J.Z.: Reference command tracking control for an air-breathing hypersonic vehicle with parametric uncertainties. J. Frank. Inst. **350**(5), 1155–1188 (2013)
40. Liu, Y.B., Xiao, D.B., Lu, Y.P.: Research on advanced fight control methods based on actuator constraints for elastic model of hypersonic vehicle. Proc. Inst. Mech. Eng. Part G. http://pig.sagepub.com/content/early/2013/08/05/0954410013498072 (2013)
41. Sun, H.B., Li, S.H., Sun, C.Y.: Adaptive fault-tolerant controller design for airbreathing hypersonic vehicle with input saturation. J. Syst. Eng. Electron. **24**(3), 488–499 (2013)
42. Farrell, J., Sharma, M., Polycarpou, M.: Backstepping-based flight control with adaptive function approximation. J. Guid. Control Dyn. **28**(6), 1089–1102 (2005)
43. Sonneveldt, L., Chu, Q.P., Mulder, J.A.: Nonlinear flight control design using constrained adaptive backstepping. J Guid. Control Dyn. **30**(2), 322–336 (2007)
44. Zong, Q., Wang, F., Tian, B.L.: Nonlinear adaptive filter backstepping flight control for reentry vehicle with input constraint and external disturbances. Proc. Inst. Mech. Eng. Part G. http://pig.sagepub.com/content/early/2013/04/05/0954410013482238 (2013)
45. Waseem, A.B., Lin, Y., Amezquita, S.K.: Adaptive dynamic surface control of a hypersonic flight vehicle with magnitude, rate and bandwidth constraints. In: Proceedings of the 18th IFAC World Congress Milano (Italy) Aug 28–Sep 2, 2011, 5341–5346
46. Waseem, A.B., Lin, Y., Amezquita, S.K.: Adaptive integral dynamic surface control of a hypersonic flight vehicle. Int. J. Syst. SCI. (2013). doi:10.1080/00207721.2013.828798
47. Xu, B., Huang, X.Y., Wang, D.W., Sun, F.C.: Dynamic surface control of constrained hypersonic flight models with parameter estimation and actuator compensation. Asian J. Control **16**(1), 1–13 (2014)
48. Waseem, A.B., Lin, Y., Amezquita, S.K.: Adaptive dynamic surface control of a hypersonic flight vehicle with improved tracking. Asian J. Control **16**(2), 1–12 (2014)
49. Zhou, Y.L., Chen, M.: Sliding mode control for NSVs with input constraint using neural network and disturbance observer. Math. Probl. Eng. **2013**, 12 (2013). Article ID 904830
50. Sigthorsson, D.O., Serrani, A.: Development of linear parameter-varying models of hypersonic air-breathing vehicles. In: AIAA Guidance, Navigation, and Control Conference. Chicago, 10–13 Aug, AIAA-2009-6282 (2009)
51. Chavez, F.R., Schmidt, D.K.: Analytical aeropropulsive/aeroelastic hypersonic-vehicle model with dynamic analysis. J. Guid. Control Dyn. **17**(6), 1308–1319 (1994)
52. Bertin, J.J., Periaux, J., Ballmann, J.: Advances in Hypersonics. BirkhÄauser, Boston (1992)
53. Schmidt, D.K., Mamich, H., Chavez, F.: Dynamics and control of hypersonic vehicles, the integration challenge for the 1990s. In: Proceedings of the 3rd International Aerospace Planes Conference, American Institute of Aeronautics and Astronautics (AIAA), Reston (1991)
54. White, D.A., Bowers, A., Iliff, K., Menousek, J.: Handbook of Intelligent Control: Neural, Fuzzy, and Adaptive Approaches, ch. Flight, Propulsion, and Thermal Control of Advanced Aircraft and Hypersonic Vehicles, pp. 357–465. Van Nostrand Reinhold, New York (1992)
55. Bolender, M.A., Doman, D.B.: Flight path angle dynamics of an air-breathing hypersonic vehicles. AIAA Guidance, Navigation, Control Conference and Exhibit, Keystone, 21–24 Aug, AIAA-2006-6692 (2006)
56. Hu, Q.L.: Robust adaptive sliding mode attitude maneuvering and vibration damping of three-axis-stabilized flexible spacecraft with actuator saturation limits. Nonlinear Dyn. **55**(4), 301–321 (2009)
57. Hu, Q.L., Xiao, B.: Fault-tolerant sliding mode attitude control for flexible spacecraft under loss of actuator effectiveness. Nonlinear Dyn. **64**(1–2), 13–23 (2011)
58. Rodriguez, A., Dickeson, J., Cifdaloz, O., Kelkar, A., Vogel, J., Soloway, D., Benavides, J., Sridharan, S.: Modeling and control of scramjet-powered hypersonic vehicles: challenges, trends, and tradeoffs. In: AIAA Guidance, Navigation and Control Conference and Exhibit, Honolulu, AIAA-2008-6793 (2008)
59. Krstic, M., Kanellakopoulos, I., Kokotovic, P.: Nonlinear and Adaptive Control Design. Wiley, New York (1995)
60. Kokotovic, P., Arcak, M.: Constructive nonlinear control: a historical perspective. Automatica **37**(2), 637–662 (2001)
61. Li, Y., Tong, S.C., Li, Y.M.: Observer-based adaptive fuzzy backstepping dynamic surface control design and stability analysis for MIMO stochastic nonlinear systems. Nonlinear Dyn. **69**, 1333–1349 (2012)
62. Swaroop, D., Hedrick, J.K., Yip, P.P., Gerdes, J.C.: Dynamic surface control for a class of nonlinear systems. IEEE Trans. Autom. Control **45**(10), 1893–1899 (2000)
63. Wang, D.: Neural network-based adaptive dynamic surface control of uncertain nonlinear pure-feedback systems. Int. J. Robust Nonlinear Control **21**, 527–541 (2011)
64. Zhao, Q.C., Lin, Y.: Adaptive dynamic surface control for pure-feedback systems. Int. J. Robust Nonlinear Control **22**, 1647–1660 (2012)
65. Park, J., Sandberg, I.W.: Universal approximation using radial-basis function networks. Neural Comput. **3**, 246–257 (1991)
66. Sanner, R.M., Slotine, J.E.: Gaussian networks for direct adaptive control. IEEE Trans. Neural Netw. **3**(6), 837–863 (1992)
67. Fei, J.T., Ding, H.F.: Adaptive sliding mode control of dynamic system using RBF neural network. Nonlinear Dyn. **70**, 1563–1573 (2012)

68. Chen, M., Ge, S.S., Ren, B.B.: Adaptive tracking control of uncertain MIMO nonlinear systems with input constraints. Automatica **47**(3), 452–465 (2011)
69. Chen, B., Liu, X.P., Liu, K.F., Lin, C.: Direct adaptive fuzzy control of nonlinear strict-feedback systems. Automatica **45**(6), 1530–1535 (2009)
70. Li, T.S., Wang, D., Feng, G., Tong, S.C.: A DSC approach to robust adaptive NN tracking control for strict-feedback nonlinear systems. IEEE Trans. Syst. Man Cybern. Part B **40**(3), 915–927 (2010)